

# **Comparative Analysis of Homeostatic Plasticity Mechanisms in Recurrent Spiking Neural Networks**

*Serenna Gerhard*



Master of Science  
School of Informatics  
University of Edinburgh  
2024

# Abstract

Hebbian plasticity alone is unable to account for stable neural function. Regulatory mechanisms are needed to maintain constancy in neuronal properties amidst Hebbian synaptic changes. Early computational schemes to constrain runaway excitation have gained strong empirical grounding, with ‘homeostatic plasticity’ now a topic of ongoing investigation. Mechanisms of homeostatic plasticity (HP) have largely been studied in isolation, and their interactions remain poorly understood. We conduct a comparative analysis across linear, non-linear, and voltage-dependent learning rules in spiking recurrent neural networks. In systematically removing HP mechanisms from each network variant, we investigate the minimal set of plasticity mechanisms required to maintain network stability and support learning under spontaneous and evoked conditions. The interactions between homeostatic and Hebbian rules are shown to have distinct impacts on network synchrony, regularity, and capacity for stimulus decorrelation. Future work should explore a minimal set of plasticity mechanisms capable of identifying higher-order statistical independence in natural scenes.

# Research Ethics Approval

This project was planned in accordance with the Informatics Research Ethics policy. It did not involve any aspects that required approval from the Informatics Research Ethics committee.

## Declaration

I declare that this thesis was composed by myself, that the work contained herein is my own except where explicitly stated otherwise in the text, and that this work has not been submitted for any other degree or professional qualification except as specified.

*(Serenna Gerhard)*

# Acknowledgements

My heartfelt gratitude to Drs Matthias Hennig and Patricia Rubisch for their curiosity, insight, and immense support throughout this project. Thank you for engaging with my ideas, for answering my many questions, and for making research a bit less intimidating. Thank you to the wonderful individuals who have made Edinburgh a second home. Thank you to everyone in Canada who has given me so much to miss, and has made me feel missed in return. Lastly, thank you to my incredible family for encouraging me to take on this adventure, and for cheering me on at every milestone. I am so fortunate to be surrounded by love 5,509 km away.

# Table of Contents

<b>1</b>	<b>Introduction</b>	<b>1</b>
<b>2</b>	<b>Background</b>	<b>3</b>
2.1	Mechanisms of homeostatic plasticity . . . . .	3
2.1.1	Synaptic scaling . . . . .	3
2.1.2	Sliding thresholds - BCM theory . . . . .	4
2.1.3	Dendritic spine size dynamics . . . . .	4
2.1.4	Rapid changes to inhibition . . . . .	5
2.1.5	Intrinsic plasticity . . . . .	5
2.2	Modelling homeostatic plasticity . . . . .	7
2.2.1	Homeostatic balance parameters . . . . .	7
2.2.2	Neuronal models . . . . .	8
2.2.3	Literature review . . . . .	8
<b>3</b>	<b>Model Specifications</b>	<b>11</b>
3.1	Network architecture . . . . .	11
3.2	Neuron and synapse model . . . . .	11
3.3	Plasticity mechanisms . . . . .	13
3.3.1	Structural plasticity . . . . .	13
3.3.2	Short-term plasticity . . . . .	13
3.3.3	Synaptic normalization . . . . .	14
3.3.4	Intrinsic plasticity . . . . .	15
3.4	Model variants . . . . .	15
3.4.1	LIF-SORN . . . . .	15
3.4.2	LIF-SORN-i . . . . .	16
3.4.3	LIF-SORN-c . . . . .	18

<b>4 Experiments</b>	<b>20</b>
4.1 Network properties . . . . .	20
4.1.1 LIF-SORN . . . . .	21
4.1.2 LIF-SORN-i . . . . .	22
4.1.3 LIF-SORN-c . . . . .	22
4.2 Plasticity mechanism knockouts . . . . .	23
4.2.1 LIF-SORN . . . . .	24
4.2.2 LIF-SORN-i . . . . .	24
4.2.3 LIF-SORN-c . . . . .	26
4.2.4 Discussion . . . . .	27
4.3 Ocular Dominance . . . . .	30
4.3.1 Baseline performance . . . . .	31
4.3.2 Plasticity mechanism knockouts . . . . .	32
4.3.3 Discussion . . . . .	34
<b>5 Conclusions</b>	<b>37</b>
<b>A Modelling Parameters</b>	<b>47</b>
<b>B Spontaneous network behaviour</b>	<b>50</b>
B.1 Baseline . . . . .	50
B.2 No synaptic normalization . . . . .	51
B.3 No intrinsic plasticity . . . . .	52
B.4 No spike-timing plasticity . . . . .	54
<b>C Evoked network behaviour</b>	<b>56</b>
C.1 Baseline . . . . .	56
C.2 No synaptic normalization . . . . .	58
C.3 No intrinsic plasticity . . . . .	60
C.4 No spike-timing plasticity . . . . .	62

# Chapter 1

## Introduction

The brain is a complex communication system. Neurons, the functional units of the brain, relay information via electrical impulses. These signals travel along neural pathways to be transmitted between neurons at specialized junctions, or synapses. At the synapse, the electrical signal triggers the release of chemical messengers which traverse the synaptic cleft and bind to postsynaptic receptors of neighbouring neurons. This process enables neurons to respond to stimuli, and forms the underlying framework for perception, cognition, and behaviour. The flow of information in the brain is therefore dictated by the structure and strength of neuronal connections.

Brain morphology is not fixed; rather, the nervous system is *plastic*, possessing the remarkable ability to modify its structural and functional connectivity in response to experience. A key component of this adaptability is synaptic plasticity, or the ability of synapses to change in strength and efficacy. Hebb (1949) introduced Hebbian learning, positing that changes in synaptic strength are driven by the coincident firing of pre- and postsynaptic neurons. Hebb proposed that if presynaptic neuron A repeatedly and persistently activates postsynaptic neuron B, neuron A will become more effective at activating neuron B in the future (colloquially, ‘neurons that fire together, wire together’). Enhancement in synaptic efficacy is termed Long-Term Potentiation (LTP). Conversely, if presynaptic neuron A’s activation is weak, infrequent, and/or poorly coordinated with the postsynaptic neuron B, synaptic strength will decrease, resulting in Long-Term Depression (LTD).

In isolation, Hebbian learning can destabilize neuronal circuitry. Consider the correlation-based rule applied to two synaptically coupled neurons: as the synapse strengthens, presynaptic neuron A increasingly drives postsynaptic neuron B, which further strengthens the synapse. This positive feedback loop may cause all synapses to

saturate or, conversely, weaken to the point of complete inactivity. A similar but distinct issue arises from fluctuations in average synaptic input. Over a neuron's lifetime, its baseline synaptic input may vary significantly due to developmental changes, such as eye-opening. Simple coincident-based synaptic modifications cannot account for how neurons avoid saturating or falling silent if average inputs rise and fall dramatically.

Therefore, Hebbian plasticity can only be effective if it operates within a framework of otherwise stable neural function. Davis (2013) writes that “without the existence of potent mechanisms that stabilize neural function, our capacity to learn and remember would be lost in the chaos of daily experiential change”. These considerations led to the augmentation of computational models to include rules which constrain runaway excitation. Early schemes were ad hoc in nature, being introduced ‘by hand’ and without a strong adherence to empirical data (Desai, 2003). However, the notion of ‘homeostatic plasticity’ has since gained a strong empirical grounding.

While recent studies have identified diverse homeostatic plasticity (HP) mechanisms, the influence of these mechanisms and their interactions is not well understood (Keck et al., 2017). Further, there is no unified investigative approach, with models within the field differing in their explanatory aims (Bredenberg & Savin, 2023). This project provides an overview of well-established HP mechanisms and traditional modelling approaches before selecting an empirically-grounded recurrent spiking neural network as a framework for further study. In investigating spontaneous activity, we gain insight into which homeostatic mechanisms are necessary or sufficient to maintain network stability. In investigating evoked activity, we gain insight into which mechanisms are necessary or sufficient to support learning.

# Chapter 2

## Background

### 2.1 Mechanisms of homeostatic plasticity

Distinct forms of homeostatic plasticity emerge repeatedly across experimental approaches (Keck et al., 2017).

#### 2.1.1 Synaptic scaling

Synaptic scaling constrains the total synaptic strength over a neuron, imposed as a function of postsynaptic activity or total synaptic efficacy. For example, the overall strength of excitatory synapses can scale up or down depending on whether average spiking activity is above or below a target value. Therefore, overall activity and total synaptic strength is kept within set bounds even while individual synaptic weights vary by Hebbian rules.

Experimental work shows neurons are indeed subject to activity-dependent rescaling of synapses. For example, the addition of pharmacological agents to neocortical neuron cultures followed by cell patch recordings show synaptic properties adapt homeostatically to prolonged exposure to different average levels of synaptic activity; neocortical pyramidal neurons up-regulate the strengths of excitatory synapses when firing rates are low, and down-regulate them when firing rates are high (Turrigiano et al., 1998). The changes in synaptic currents are attributed to changes in the number of receptors at each synapse, namely AMPA glutamate receptors at excitatory synapses (Desai, 2003).

Synaptic scaling develops slowly and cumulatively, with several hours of manipulation required to produce measurable changes (Turrigiano, 1999). This indicates neurons

can integrate activity over time, rather than responding to activity moment to moment. Further, scaling is global and (generally) multiplicative, meaning all synaptic weights on an individual neuron are modified by a single multiplicative scaling factor. Thus, scaling controls total activation while preserving relative differences between synapses. These characteristics enable synaptic scaling to work concurrently with Hebbian learning.

### **2.1.2 Sliding thresholds - BCM theory**

BCM models alter a synapse's capacity for Hebbian modification via an activity-dependent sliding threshold. This scheme was popularized by Bienenstock, Cooper, and Munro (BCM), whose learning rule is commonly used to describe the dynamic adjustment of thresholds over time (Bienenstock et al., 1982). The change in the efficacy of a synapse depends on a slowly varying time-averaged value of postsynaptic activity, in addition to instantaneous pre- and postsynaptic activities.

Under BCM theory, whether individual synapses are strengthened or weakened by presynaptic activity depends on whether postsynaptic activity is above or below a threshold firing rate. The threshold rate, a crossover point between potentiation and depression, is itself a slow function of postsynaptic activity. It functions to make potentiation more likely when average activity is low, and depression when activity is high (Toyoizumi et al., 2014).

Experimental evidence for BCM theory was obtained by dark rearing rats, and comparing their retinal ganglion firing to those of rats raised under normal lighting conditions (Kirkwood et al., 1996). As predicted by the BCM rule, low activity in dark-reared conditions eased the induction of potentiation and challenged the induction of depression. There is no consensus on the biological basis of the sliding threshold, and several mechanisms have been proposed (Fox & Stryker, 2017). BCM theory is extensively reviewed by (Cooper & Bear, 2012).

### **2.1.3 Dendritic spine size dynamics**

Dendrites extend outward from a neuron's cell body to receive incoming information. In the mammalian brain, most excitatory synapses are located on small protrusions arising from dendrites - termed dendritic spines - which act as electrically isolated micro-compartments. Spines exhibit both structural and functional plasticity in response to modified input activity.

It has been shown that dendritic spine size is tightly correlated with synaptic strength

and that spine size is regulated during synaptic plasticity (Bosch et al., 2014). Spine morphology is hypothesized to relate to synaptic plasticity via the regulation of  $\text{Ca}^{2+}$ , where  $\text{Ca}^{2+}$  initiates a biochemical cascade in spine machinery which contributes to LTP or LTD of the synapse (Suratkal et al., 2021). Biophysical models of pyramidal neurons show agreement that spines enlarge during LTP and shrink during LTD (Keck et al., 2017). Further, simulation studies of recurrent networks indicate that fluctuations in spine size help stabilize network activity by maintaining a spine size distribution close to the physiological steady-state distribution, while Hebbian plasticity forms and maintains cell assemblies (Loewenstein et al., 2011).

#### **2.1.4 Rapid changes to inhibition**

The homeostatic mechanisms discussed above operate on slow timescales, from a period of hours to days, and are too slow to account for activity peaks which may lead to pathological over-excitation (Turrigiano, 2017). In contrast, Hebbian plasticity can occur on the order of seconds to minutes. Although it is possible to artificially adjust the timescales of these learning rules to meet the demands of network stability, rapid mechanisms with biological groundings have also been investigated. One such mechanism involves altering the activity of inhibitory neurons. Globally balanced neuronal networks display approximately equal amounts of de- and hyperpolarizing membrane currents. It is believed that synaptic plasticity at inhibitory synapses plays a central role in maintaining this balance.

Monocular deprivation *in vivo* studies indicate rapid disinhibition within cortical circuitry occurs after sensory deprivation (Gainey & Feldman, 2017). Disinhibition is likely mediated by NMDA receptor downregulation, confirmed by physiological studies in slices of prefrontal cortex from rats treated with an NMDAR antagonist (Zhang et al., 2008). The antagonist produced biochemical changes to the GABA system, resulting in both reduced amplitude and frequency of inhibitory currents, and increased postsynaptic excitability. Increased excitability can be properly attributed to the disinhibition as postsynaptic current properties and intrinsic excitability were not changed.

#### **2.1.5 Intrinsic plasticity**

Focusing solely on changes to synaptic strength provides an incomplete window into the evolution of neural dynamics; the intrinsic electrical properties of individual neurons can also be modified by experience. How a neuron integrates synaptic input is regulated

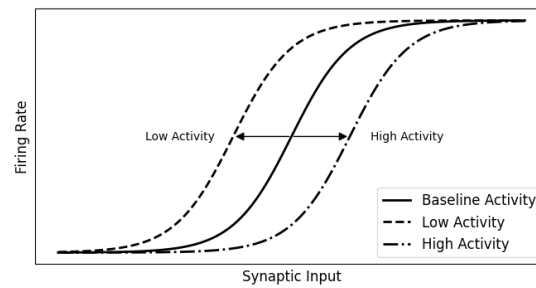


Figure 2.1: How intrinsic plasticity might adapt neuronal firing to changes in synaptic input. Recreated from Desai (2003).

by its distribution of intrinsic ion channels. Altering the magnitude and/or distribution of intrinsic channels implicates diverse processes including the pattern and rate of firing, neuronal excitability, and synaptic integration and plasticity (Desai, 2003).

Intrinsic plasticity theory postulates that neurons adapt to changes in activity by altering how synaptic inputs are transformed into firing rates. This is modelled by a  $f-I$  curve, relating a neuron's outputted firing rate to the synaptic input it receives, as shown in Figure 2.1. At low inputs the neuron will not fire. Likewise, at high inputs the firing rate will plateau, indicating a saturation point where, despite further increases in input, the firing rate cannot increase due to biophysical limits. The linear region indicates where the neuron's firing is sensitive to changes in input. If synaptic input decreases, the curve shifts left to prevent the neuron falling silent. Conversely, the curve shifts right in response to very high input to prevent saturation. In general, the  $f-I$  should shift such that the sensitive linear region corresponds with the average input level.

Neocortical cultures were observed after the addition of pharmacological agents to evoke low or high firing, confirming the presence of IP in homeostatic regulation (Desai, 2003). The experiments showed pyramidal neurons responded to periods of prolonged activity deprivation by increasing their intrinsic excitability (by becoming 'easier to fire'). The changes in excitability can be attributed to coordinated changes in the density of intrinsic channel types. Interestingly, the manipulation did not have global effects on intrinsic currents but rather selectively and coordinately altered the ratio of inward and outward currents. Therefore, voltage-gated channels are not regulated in isolation but synergistically such that their combined effort produces the desired firing rate.

## 2.2 Modelling homeostatic plasticity

### 2.2.1 Homeostatic balance parameters

Homeostatic mechanisms are required to restore cellular and synaptic activity following perturbations. In each of the mechanisms described above, HP works to restore a parameter of neuronal circuitry. O’Leary and Wyllie (2011) propose homeostatic compensation exemplifies principles of control theory, highlighting the potential for modelling efforts to depict HP mechanisms in a feedback control system. In particular, this perspective allows the differentiation between long-term changes to homeostatic targets, and on-going adjustments in response to Hebbian perturbations.

Experimental evidence is documented for three homeostatic balance parameters; firing rate, sub-threshold activity, and synaptic weights. Fox and Stryker (2017) suggest that, when incorporated in an appropriate theoretical model, any of these parameters may stabilize the network away from pathological dynamics. The concept of firing rate homeostasis was first observed alongside the discovery of synaptic scaling (Turrigiano et al., 1998). Subsequent research has consistently shown altering both cellular (Burrone et al., 2002) and network (Desai et al., 2002) firing rates induces homeostatic mechanisms. Both *in vitro* and *in vivo* studies have demonstrated that neurons recover set-point firing rates in parallel with the activation of homeostatic mechanisms (Hengen et al., 2013). BCM theory supports homeostatic modulation of firing rates, as does intrinsic plasticity paradigms. More recently, Fong et al. (2015) found that sub-threshold changes were sufficient to induce synaptic scaling. This parameter is relatively unexplored - it has not been shown whether sub-threshold changes restore activity levels (Fox & Stryker, 2017). Synaptic weight homeostasis is presented as an alternative to homeostatic regulation of firing rates (Davis & Bezprozvanny, 2001). Bourne and Harris (2011) hypothesize that overall synaptic weight is conserved on a dendritic branch to prevent hyperactivity resulting from the over-strengthening of synapses.

This summary presents a somewhat oversimplified picture of homeostatic balance parameters. Empirical studies find significance variability; it may be that there is no simple homeostatic ‘target’ that the networks try to maintain, but rather some *other* functionally relevant aspect. Hennig et al. (2011) found that networks try to maintain population dynamics. In computational simulations, the homeostatic target is largely determined by the level of detail in the model selected for inquiry.

### 2.2.2 Neuronal models

Neuron models simplify and abstract the process of neuronal communication. Neuron models can be classified by level of biological detail into rate, spiking and biophysical models. Rate models describe neuronal activity in terms of average firing rates over time, rather than individual spikes. They simplify the complexity of spike timing and are therefore more computationally efficient but lacking temporal precision. For example, the Wilson-Cowan model describes the dynamics of excitatory and inhibitory populations in terms of their average firing rates (Wilson & Cowan, 1972).

Spiking models simulate the precise timing of action potentials (spikes), capturing the detailed temporal dynamics of individual neurons. Spiking models are more computationally demanding as they require the integration of differential equations which govern synaptic membrane potential over time. The leaky integrate-and-fire (LIF) model is a popular spiking paradigm, which models input integration until a threshold is reached, triggering a spike.

Biophysical models are the most complex of neuron model classes. They aim to accurately simulate the biological processes underlying neuronal activity by modelling the activity of ion channels which alter synaptic membrane potentials. The Hodgkin-Huxley model is the prototypical biophysical model, describing how action potentials are generated by the dynamics of sodium and potassium channels. Biophysical models may also simulate neurons with multiple compartments (e.g., dendrite, soma, axon) to capture spatial dynamics in neuronal signalling. Predictably, these models require significant computational resources.

### 2.2.3 Literature review

The vast array of model types, target parameters, learning rules, and homeostatic mechanisms can be overwhelming. To aid in the synthesis of existing knowledge, Table 2.1 compiles publications which develop a model of a homeostatic plasticity mechanism alone, or integrated with a form of Hebbian learning in a neuronal network.

Paper	Model Type	Plasticity	Balance Parameter(s)
von der Malsburg, 1973	Rate	Hebbian correlation-based synaptic plasticity, synaptic normalization (SN)	Firing rate

Paper	Model Type	Plasticity	Balance Parameter(s)
Miller and MacKay, 1994	Mathematical	Hebbian correlation-based synaptic plasticity, multiplicative and subtractive SN	Synaptic weight
Lazar et al., 2009	Spiking	Spike-timing dependent plasticity (STDP), SN, intrinsic plasticity (IP)	Firing rate
Litwin-Kumar and Doiron, 2014	Spiking	Voltage-dependent STDP, inhibitory synaptic plasticity (iSTDP), subtractive SN	Firing rate
Zenke et al., 2013	Spiking	'Metaplastic' triplet-STDP, SN	Firing rate
Elliott and Shadbolt, 2002	Mathematical	Non-linear Hebbian growth rule, "emergent" multiplicative SN	Energy minimization
Wu and Yamaguchi, 2006	'Phase'/spiking	Asymmetrical STDP. Regulates saturation level (maximum synaptic weight) and learning rate (synaptic plasticity speed)	Firing rate
Finelli et al., 2008	Biophysical	STDP, spike-rate dependent timing (SRDP)	Specificity of Kenyon cells to meaningful odors (KC targets)
Chen et al., 2013	Biophysical	Postsynaptic energy potential expresses changes in synaptic weights	Metabolic energy
Kempter et al., 1999	Spiking	Asymmetric STDP	Spike-spike correlations
Soures et al., 2017	Spiking	STDP, SN, IP	Firing rate, threshold voltage
Tetzlaff et al., 2011	Rate	Hebbian and Anti-Hebbian learning, SN (weight-independent, linear weight dependence, and non-linear weight dependence)	Firing rate
Toyoizumi et al., 2013	Rate	Synaptic strength is the product of synapse-specific Hebbian factor and a postsynaptic-cell-specific homeostatic factor, BCM rule, multiplicative SN	Firing rate
Sweeney et al., 2015	Biophysical	STDP, diffusive and non-diffusive homeostasis	Firing rate

Paper	Model Type	Plasticity	Balance Parameter(s)
Xu et al., 2024	Spiking	Short-term plasticity (STP), experience-dependent adaptive SN	Gradient signals regulated by a corresponding scaling factor
Benuskova and Abraham, 2007	Spiking	STDP with BCM sliding threshold	Firing rate
Pfister and Gerstner, 2006	Spiking	Triplet STDP	Firing rate
Shouval et al., 2002	Biophysical	STDP, calcium levels alters firing threshold (IP)	Firing rate
Abbott et al., 1997	Spiking	Inhibition/internal plasticity; short-term dynamic depression provides an automatic, dynamic gain-control mechanism	Firing rate
Koulakov et al., 2009	Mathematical	Multiplicative Hebb-like learning rule, re-normalization of the principle eigenvalue (equivalent to SN)	Firing rate distribution, synaptic strength distribution
Mongillo et al., 2018	Spiking	Hebbian and anti-Hebbian learning rules, IP	Firing rate distribution
Papa et al., 2017	Spiking	STDP, structural plasticity, inhibitory STDP, SN, IP	Firing rate

Table 2.1: Snapshot of Hebbian and homeostatic plasticity modelling efforts to date.

Table 2.1 is not a comprehensive resource; rather, it can be considered a ‘snapshot’ into the field. It confirms homeostatic targets are dependent on the level of biophysical detail included in network composition. For example, Sweeney et al. (2015) develop a model of homeostatic control which balances levels of nitric oxide, a gaseous signalling molecule omitted in more abstract neuron models. The number of biophysical models increase in recent years, often building on rate models by reformulating the learning rules within a biologically plausible context. However, firing rate remains the most prevalent homeostatic balance parameter across model types.

In their review, Keck et al. (2017) identify that the field would benefit from tighter interactions between theoreticians and experimentalists, with a focus on detailed mechanistic work. Several researchers are shown to emulate this approach. For example, Chen et al. (2013) conduct *in vitro* experiments of pyramidal cells from rat visual cortices and develop a cortical neuron model with properties matching their experimental data.

# Chapter 3

## Model Specifications

The following experimental work explores three recurrent spiking neural networks, each integrating a Hebbian learning rule with prototypical homeostatic mechanisms. The networks share a common base architecture, adapted from Klos et al. (2018), and publicly available at <https://github.com/chklos/lifsorn-seqlearn>. All simulations were performed using Python, leveraging the Brian simulator developed for modelling spiking neural networks (Brian2, 2024). All parameters used in simulations are available in Appendix A.

### 3.1 Network architecture

The base model, developed by Miner and Triesch (2016) and adapted by Klos et al. (2018), is a recurrent spiking neural network representing a small rectangular grid of L5 rodent visual cortex. The model consists of  $N^E = 1000$  excitatory and  $N^I = 0.2 \times N^E = 200$  inhibitory leaky integrate-and-fire neurons with conductance-based synapses and Gaussian membrane noise. The  $2500 \mu\text{m} \times 1000 \mu\text{m}$  grid is randomly populated by neurons with distance-dependent connectivity, where a neuron is more likely to connect with neighbouring neurons than with distant neurons, in accordance with experimental data (Song et al., 2005). Distance-dependent connectivity for arbitrary excitatory neuron  $n_e$  is shown in Fig 3.1.

### 3.2 Neuron and synapse model

The membrane potential  $V_n$  of neuron  $n$  evolves according to subthreshold leaky integrate-and-fire dynamics governed by

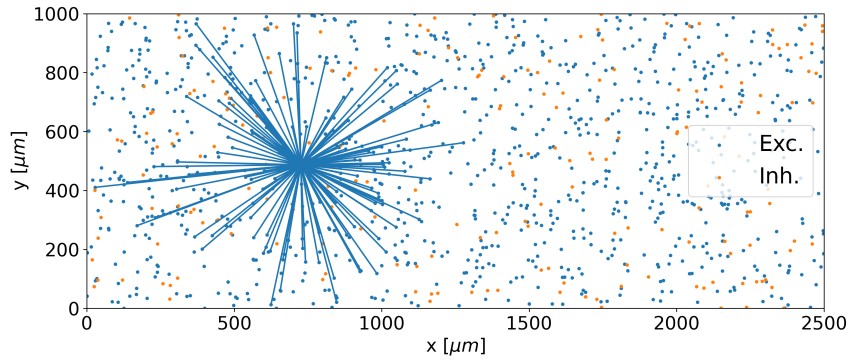


Figure 3.1: Distribution of neurons on the 2D. Blue lines show all connections projecting from an excitatory neuron  $n_e$ .

$$\begin{aligned} \frac{dV_n}{dt}(t) = & -\frac{V_n(t) - E_L}{\tau} \\ & - \frac{(g_{e,n}(t) + g_{\text{ext},n}(t))(V_n(t) - E_e)}{\tau} \\ & - \frac{g_{i,n}(t)(V_n(t) - E_i)}{\tau} + \frac{\sigma\zeta(t)}{\sqrt{\tau}} \end{aligned} \quad (3.1)$$

where  $\frac{dV_n}{dt}(t)$  is the rate of change of the membrane potential  $V_n$  with respect to time,  $E_L$  is the resting potential,  $g_{e,n}(t)$  is the excitatory synaptic conductance,  $g_{\text{ext},n}(t)$  is the external synaptic conductance,  $E_e$  is the excitatory reversal potential,  $g_{i,n}(t)$  is the inhibitory synaptic conductance,  $E_i$  is the inhibitory reversal potential,  $\zeta_x(t)$  is Gaussian white noise,  $\sigma(t)$  is the standard deviation of the Gaussian noise, and  $\tau$  ms is the membrane time constant. Recurrent excitatory synapses are subject to synaptic plasticity, with excitatory synaptic conductance is determined by

$$\frac{dg_{e,n}}{dt}(t) = \frac{g_{e,n}(t)}{\tau_e} + \sum_{m_e} W_{m_e n}^{\text{eff}}(t) \sum_{f_{m_e}} \delta(t - t_{f_{m_e}} - t_{m_e n}) \quad (3.2)$$

where  $\frac{dg_{e,n}}{dt}(t)$  is the rate of change of the excitatory synaptic conductance  $g_{e,n}$  with respect to time,  $\tau_e$  is the synaptic time constant for excitatory connections,  $W_{m_e n}^{\text{eff}}(t)$  is the dimensionless effective connection weight between neuron  $m_e$  and neuron  $n$ ,  $t_{m_e n}$  is the conduction delay between neuron  $m_e$  and neuron  $n$ , and  $f_{m_e}$  indexes the spike times

of neuron  $m_e$ . Inhibitory synaptic conductance is governed by

$$\frac{dg_{i,n}}{dt}(t) = \frac{g_{i,n}(t)}{\tau_i} + \sum_{m_i} W_{m_i n} \sum_{f_{m_i}} \delta(t - t_{f_{m_i}} - \tau_{m_i n}) \quad (3.3)$$

where  $\frac{dg_{i,n}}{dt}(t)$  is the rate of change of the inhibitory synaptic conductance  $g_{i,n}$  with respect to time,  $\tau_i$  is the synaptic time constant for inhibitory connections,  $W_{m_i n}(t)$  is the connection weight between neuron  $m_i$  and neuron  $n$ ,  $t_{m_i n}$  is the conduction delay between neuron  $m_e$  and neuron  $n$ , and  $f_{m_i}$  indexes the spike times of neuron  $m_i$ . When the membrane potential rises above a threshold potential ( $V_i V_t$ ), the neuron model fires a spike and the membrane threshold is returned to a reset potential.

### 3.3 Plasticity mechanisms

#### 3.3.1 Structural plasticity

Structural plasticity functions via two network operations which grow new and prune weak recurrent excitatory connections. Synaptic growth is implemented by adding a random number of synaptic connections once per simulation second with weak initial weightings, while synaptic pruning is modelled by eliminating all connections whose weight falls below a set threshold once per second. Synaptic growth and pruning function to achieve a target recurrent excitatory network sparsity.

Recurrent excitatory connections are assigned a probability according to their distance from neuron  $n_e$ , determined from a Gaussian probability function with a mean of  $0\mu m$  and a half width of  $200\mu m$ , and drawn from this distribution to determine new synapse growth. Connections are populated and pruned throughout a 400s ‘growth’ phase, during which sparsity reaches an equilibrium at target value. Sparsity parameters are in agreement with experimentally observed values of the L5 of the rodent cortex (Thomson et al., 2002).

#### 3.3.2 Short-term plasticity

Short-term plasticity (STP) modulates  $W_{m_e n_e}(t)$  depending on the short-term firing history of the presynaptic neuron  $m_e$ . Short-term facilitation  $u_{m_e}(t)$  dynamics are governed by

$$\frac{du_{m_e}}{dt}(t) = \frac{U - u_{m_e}(t)}{\tau_f} + U(1 - u_{m_e}(t)) \sum_{f_{m_e}} \delta(t - t_{f_{m_e}} - t_{ee}) \quad (3.4)$$

where  $t_{ee}$  is the conduction delay between excitatory neurons,  $U$  is the increment of  $u_{m_e}(t)$  produced by a presynaptic spike,  $\tau_f$  is the facilitation timescale,  $f_{m_e}$  indexes the presynaptic spikes, and  $t^-$  indicates the time prior to spike arrival at the synapse. The first term  $\frac{U-u_{m_e}(t)}{\tau_f}$  describes the gradual return of  $u_{m_e}(t)$  to its baseline value  $U$  over time. The second term  $U(1-u_{m_e}(t))\sum_{f_{m_e}}\delta(t-t_{f_{m_e}}-t_{ee})$  represents the instantaneous change to  $u_{m_e}(t)$  when a presynaptic spike arrives at the synapse. Likewise, depression  $x_{m_e}(t)$  dynamics evolve according to

$$\frac{dx_{m_e}}{dt}(t) = \frac{1-x_{m_e}(t)}{\tau_d} + x_{m_e}(t)u_{m_e}(t)\sum_{f_{m_e}}\delta(t-t_{f_{m_e}}-t_{ee}) \quad (3.5)$$

The effective connection weight when a spike arrives at a synapse is therefore determined by

$$W_{m_e n_e}^{eff}(t) = W_{m_e n_e}(t) \times u_{m_e}(t) \times x_{m_e}(t) \quad (3.6)$$

STP will temporarily decrease synaptic strength after repeated spikes at presynaptic neuron. The mechanism of STP synaptic depression may be motivated by a depletion of resources necessary for transmission at the synapse; if the presynaptic neurons fires repeatedly in quick succession, resources are used faster than they can be replenished, leading to progressive reduction in the availability of vesicles. This process is captured by a decrease in  $x_{m_e}$ .

### 3.3.3 Synaptic normalization

Synaptic normalization (SN) scales the total synaptic drive such that the total incoming weight for each excitatory neuron is constant. It updates all recurrent excitatory weights once per second according to

$$W_{m_e n_e}(t) \rightarrow W_{total}(n_e) \frac{W_{m_e n_e}(t)}{\sum_{m_e} W_{m_e n_e}} \quad (3.7)$$

where  $W_{total}(n_e)$  is the target total input for  $n_e$ .  $W_{total}(n_e)$  is calculated by multiplying the size of the incoming neuron population by a sparsity parameter, the mean synapse strength, and  $Z$ , the integral of a normal distribution centered at the neuron's position over the network distribution

$$Z = \int_{2500 \text{ mm}}^{0 \text{ mm}} dx \int_{1000 \text{ mm}}^{0 \text{ mm}} dy \frac{1}{2\pi\sigma^2} \exp\left(-\frac{(x-x_{n_e})^2 + (y-y_{n_e})^2}{2\sigma^2}\right) \quad (3.8)$$

where  $x_{n_e}$  is the position of neuron  $n_e$  and  $\sigma$  is the half-width of the Gaussian probability function.  $Z$  is used to assign distance-dependent probability to each possible

connection, accounting for the increased number of connections formed by central neurons versus neurons close to the grid boundaries. That is, without  $Z$  mean weights of connections projecting to peripheral neurons would be higher than mean weights of connections projecting to central neurons. Other connection types are similarly normalized prior to simulation runtime.

### 3.3.4 Intrinsic plasticity

Intrinsic plasticity (IP) regulates the firing threshold  $V_{T,n_e}(t)$  of each excitatory neuron  $n_e$ . The threshold is updated at every simulation time-step according to

$$V_{T,n_e}(t) \rightarrow V_{T,n_e}(t) + \eta_{IP}(N_{spikes} - h_{IP}) \quad (3.9)$$

where  $N_{spikes} = 1$  if  $n_e$  spiked in the previous time-step and 0 otherwise,  $\eta_{IP}$  is the learning rate,  $h_{IP} = r_{target} * \Delta t_{sim}$  is the target number of spikes per update interval, and  $r_{target}$  is the target firing rate. IP differs from the other plasticity mechanisms in that it stabilizes network activity at the level of the individual neuron. However, the mechanism is simplistic as it assigns the same target firing rate to each neuron. IP conceptually functions in the same manner as the biologically observed spike-rate adaptation, which reduces neural firing in response to continuous input.

## 3.4 Model variants

### 3.4.1 LIF-SORN

In the leaky integrate-and-fire self-organizing neural network (LIF-SORN) base model, neurons modify their synaptic strength according to a simple spike-timing-dependent plasticity (STDP) rule, which modifies the synaptic weight  $W_{m_e n_e}(t)$  between excitatory neurons  $m_e$  and  $n_e$  according to

$$\Delta W_{m_e n_e} = \sum_{f_{m_e}} \sum_{j_{n_e}} W(t - t_{f_{m_e}} - t_{ee}) \quad (3.10)$$

$f_{m_e}$  indexes the presynaptic spikes,  $j_{n_e}$  indexes the postsynaptic spikes, and  $t_{ee}$  is the conduction delay between excitatory neurons. This equation sums the contributions of all presynaptic and postsynaptic spike pairs, adjusted by the STDP window function. The STDP window function determines the weight change based on the timing

difference  $\Delta t = t - t_{f_{me}} - t_{ee}$  as follows

$$W(\Delta t) = \begin{cases} A_+ \exp\left(-\frac{\Delta t}{\tau_+}\right) & \text{if } \Delta t > 0 \\ A_- \exp\left(\frac{\Delta t}{\tau_-}\right) & \text{if } \Delta t < 0 \\ 0 & \text{if } \Delta t = 0 \end{cases} \quad (3.11)$$

where  $A_+$  and  $A_-$  are potentiation and depression amplitudes, and  $\tau_+$  and  $\tau_-$  are time constants for potentiation and depression.

### 3.4.2 LIF-SORN-i

The notation used to describe the LIF-SORN STDP mechanism obscures some relevant computational details. Directly simulating equation 3.10 - by summing over all pairs of spikes - is both inefficient and physiologically unrealistic. A more practical approach involves defining ‘traces’ of pre- and postsynaptic activity. This formulation relies on the assumption that the arrival of the spike at a synapse leaves a trace of some quantity which decays exponentially over time. This could be interpreted as the quantity of neurotransmitter which is bound to postsynaptic receptors.

When a presynaptic spike occurs before a postsynaptic spike, the change in weight is proportional to an amplitude parameter ( $A_+$ ) and the value of the presynaptic trace at the moment of the postsynaptic spike, which decays according to  $\tau_+$ . Likewise, when a postsynaptic spike occurs before a presynaptic spike, the change in weight is proportional to an amplitude parameter  $A_-$ , and the value of the postsynaptic trace at the moment of the presynaptic spike, which decays according to  $\tau_-$ . The decay of the synaptic traces is described by the differential equations:

$$\tau_+ \frac{d}{dt} a_{m_e}^+ = -a_{m_e}^+ + \delta(t - t_{m_e}) \quad (3.12)$$

$$\tau_- \frac{d}{dt} a_{n_e}^- = -a_{n_e}^- + \delta(t - t_{n_e}) \quad (3.13)$$

Integrating the differential equation results in standard exponential functions

$$a_{m_e}^+(t) = \exp\left(-\frac{\Delta t}{\tau_+}\right) \quad \text{for } t > t_{m_e} \quad (3.14)$$

$$a_{n_e}^-(t) = \exp\left(\frac{\Delta t}{\tau_-}\right) \quad \text{for } t > t_{n_e} \quad (3.15)$$

Therefore the total weight change is calculated:

$$\frac{d}{dt}w_{m_e n_e} = A_{pre}a_{m_e}^+\delta(-\Delta t) + A_{post}a_{n_e}^-\delta(\Delta t)$$

where the weight change is a linear sum of the traces evaluated at the time of the secondary spike, multiplied by the corresponding amplitude parameter. In their implementation, Klos et al. (2018) encode the trace update equal to the amplitude of potentiation or depression:

$$a_{m_e}^+ = A_+ \quad \text{and} \quad a_{n_e}^- = A_- \quad (3.16)$$

This results in a rapidly fluctuating trace, show in Figure 3.2. We alter trace encoding to allow incremental trace updates according to:

$$a_{m_e}^+ = a_{m_e}^+ + A_+ \quad \text{and} \quad a_{n_e}^- = a_{n_e}^- + A_- \quad (3.17)$$

This adjustment enables trace behaviour to accumulate, shown in Figure 3.3.

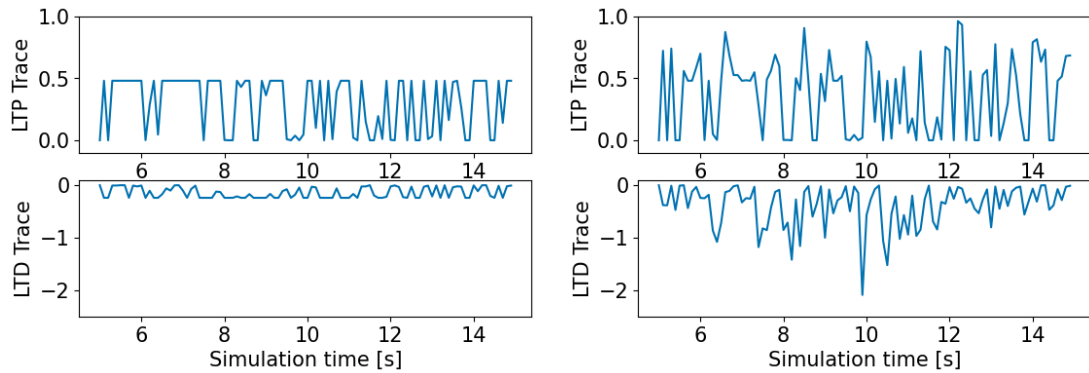


Figure 3.2: LIF-SORN LTP and LTD traces. Figure 3.3: LIF-SORN-i LTP and LTD traces

This modification has interesting implications for network dynamics. When traces  $a_{m_e}^+$  and  $a_{n_e}^-$  are reset to a fixed value ( $A_+$  or  $A_-$ ) upon each spike pair event, the synaptic weight change depends only on the most recent spike timing. When traces are allowed to accumulate, the weight change depends upon a sum of contributions from multiple spike pair events. This model can be tied to empirical work demonstrating that in visual cortical slices, the contribution of each spike pair to synaptic modification depends not only on the interval between the pair, but also on the timing of preceding spikes (Froemke & Dan, 2002).

### 3.4.3 LIF-SORN-c

The simple STDP learning rules introduced above have been critiqued as insufficient in capturing all the necessary factors required to induce Hebbian learning in relying solely on the temporal window in which spiking occurs. Rather, the requirement for synaptic modification may be ‘protected’ by multiple conditions which must be met before weights can be persistently altered (Lisman & Spruston, 2005). Empirical study shows that LTD versus LTP induction depend on the level of depolarization of the postsynaptic membrane, indicating a complex relationship between rate and timing not captured by classical STDP (Artola et al., 1990).

Clopath et al. (2010) propose a model of spike-timing-dependent plasticity in which synaptic changes are influenced by the postsynaptic membrane potential  $s(t)$ . Their modelling efforts successfully reproduce biological phenomena which cannot be accounted for in traditional models of STDP. This approach has been highlighted as a promising area for future research by Miner and Triesch (2016) and has also been investigated by (Rubisch, 2024). The voltage-dependent learning mechanism proposed by Clopath et al., 2010 was integrated into the LIF-SORN, replacing the classical STDP mechanism.

Voltage-based models compute changes in synaptic weight by comparing a voltage variable against depression and potentiation thresholds. To remain consistent with a large body of experimental data which indicates that synaptic depression and potentiation occur via distinct pathways, Clopath et al. (2010) use separate additive contributions to the plasticity rule for LTD versus LTP. LTD is triggered if presynaptic spike arrival occurs while the membrane potential of the postsynaptic neuron is slightly depolarized (above a threshold  $\theta_-$ ), while LTP occurs if the postsynaptic membrane potential is substantially depolarized (above a second threshold  $\theta_+$ ). Mathematically, the plasticity rule differentiates momentary voltage  $s$  and low-pass filtered voltage variables  $\bar{s}_-$  and  $\bar{s}_+$ , denoting temporal averages over recent synaptic history.

#### 3.4.3.1 LTD

Presynaptic spike arrival at neuron  $n_e$  from neuron  $m_e$  depresses the synaptic weight  $W_{m_e n_e}(t)$  proportional to the average postsynaptic depolarization  $\bar{s}_-(t)$  according to

$$\tau_- \frac{d}{dt} \bar{s}_-(t) = \bar{s}_-(t) + s(t) \quad (3.18)$$

$\bar{s}_-(t)$  is a low-pass filtered version of the post-synaptic membrane potential with a time constant  $\tau_-$ . Synaptic depression is therefore modelled as

$$\Delta W_{m_e n_e}^-(t) = -A_{LTD} X_{n_e}(t) [\bar{s}_-(t) - \theta_-]_+ \quad \text{if } w_{n_e} < w_{min} \quad (3.19)$$

where  $A_{LTD}$  is a constant amplitude parameter,  $X_{n_e} = \sum_n \delta(t - t_{n_e}^n)$  describes spike train at the synapse,  $n_e$  is the index of the synapse and  $n$  is an index that counts the spike, and  $[\ ]_+$  brackets indicate a rectification filter such that any value  $\bar{s}_- < \theta_-$  does not cause synaptic depression. Rectification ensures that postsynaptic depolarization must exceed a threshold  $\theta_-$  to establish synaptic depression, in agreement with experimental findings (Gerstner & Kistler, 2002). Therefore, LTD occurs if the average voltage of  $\bar{s}_-$  is above rest ( $w_{min} = 0$ ) at the moment of presynaptic spike arrival.

### 3.4.3.2 LTP

The LTP synaptic trace  $\bar{x}_{n_e}(t)$  decays exponentially in the absence of presynaptic spikes, with temporal dynamics described by

$$\tau_x \frac{d}{dt} \bar{x}_{n_e}(t) = -\bar{x}_{n_e} + X_{n_e}(t) \quad (3.20)$$

where  $X_{n_e}$  is the spike train, and  $\tau_x$  is the time constant of the exponential decay. Potentiation of  $W_{m_e n_e}(t)$  is proportional to trace  $\bar{x}_{n_e}(t)$  according to

$$\frac{d}{dt} W_{n_e}^+(t) = A_{LTP} \bar{x}_{n_e}(t) [s(t) - \theta_+]_+ [\bar{s}_+(t) - \theta_-]_+ \quad \text{if } w_{n_e} < w_{max} \quad (3.21)$$

where  $\bar{s}_+$  is another low-pass filtered version of  $s(t)$  with a shorter time constant  $\tau_+$  than  $\bar{s}_-$ . Potentiation therefore occurs if a) the momentary voltage  $s(t)$  is above the threshold  $\theta_+$  (this condition is fulfilled during action potential firing) b) the average voltage  $\bar{s}_+(t)$  surpasses the threshold  $\theta_-$  (fulfilled if there has been a depolarization in the recent past) and c) the trace  $\bar{x}$  from a previous presynaptic event is nonzero (fulfilled when a presynaptic spike arrived at the synapse a few milliseconds previously). Combined, the weight update rule can be written

$$\frac{d}{dt} W_{n_e}(t) = -A_{LTD} X_{n_e}(t) [\bar{s}_-(t) - \theta_-]_+ + A_{LTP} \bar{x}_{n_e}(t) [s(t) - \theta_+]_+ [\bar{s}_+(t) - \theta_-]_+ \quad (3.22)$$

if  $0 < w_{n_e} < w_{max}$

# Chapter 4

## Experiments

### 4.1 Network properties

In the absence of external stimuli, cortical networks exhibit asynchronous irregular spiking (Cooper et al., 2004). Synchrony refers to the joint spiking of neurons and is quantified by the pairwise correlation coefficient between neurons  $m$  and  $n$ :

$$c_{mn} = \frac{\text{cov}(C_m, C_n)}{\sqrt{\text{Var}(C_m)\text{Var}(C_n)}} \quad (4.1)$$

where  $C_m$  is the time series of spike counts of neuron  $m$ . The pairwise (or Pearson) correlation coefficient ranges from -1 to 1, where  $c_{mn} = 1$  indicates a perfect positive correlation where neurons fire in a synchronized manner and  $c_{mn} = 0$  indicates no linear correlation, or no firing pattern synchrony. Regularity describes the variability of spiking of individual neurons. The Poisson process is well-suited for modeling irregular spiking, not accounting for a neuron's refractory period (Abbott & Dayan, 2001). In a Poisson process, the time between consecutive events - or interspike interval (ISI) - follows an exponential distribution, and the coefficient of variation (CV) - measuring the variability in the number of events relative to the mean number of events - is 1.

Prior to exploratory simulations, the LIF-SORN was reduced ten-fold to ease computational expense and increase the number of simulations that could be run. The network growth phase was abstracted out such that the network could be initialized with post-growth recurrent excitatory weights, and the magnitude of synaptic weights were increased tenfold to account for decreased connectivity in the reduced network. To validate that the network retained asynchronous irregular firing, basic network properties of the original ( $N^E = 1000$ ) and reduced ( $N^E = 100$ ) networks were characterized in the absence of external input.

### 4.1.1 LIF-SORN

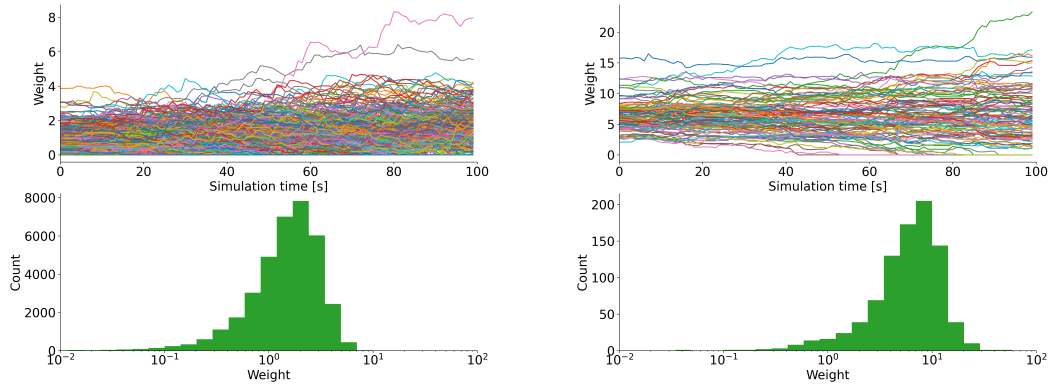


Figure 4.1: LIF-SORN recurrent excitatory weight dynamics (top) and final distributions (bottom).  $N^E = 1000$  left,  $N^E = 100$  right.

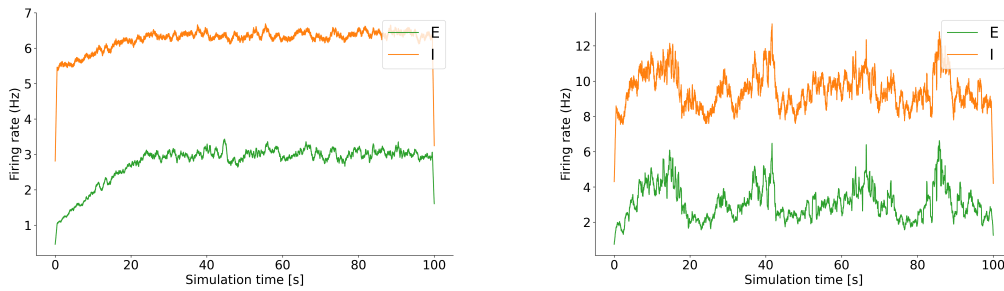


Figure 4.2: Population firing rates across model size.  $N^E = 1000$  left,  $N^E = 100$  right.

The networks operate in a fluctuation-driven regime, marked by a balance in excitatory and inhibitory inputs such that the mean membrane potential fluctuates below firing thresholds. Activity is driven by random variation about the mean, characterized by low firing rates, irregular spiking, and lognormal weight distributions (Petersen & Berg, 2016). Shown in Figure 4.2, reducing the size of the network results in a shift in the firing rates and oscillatory behaviour of the neuron populations. Slow oscillatory behaviour is introduced to the average population firing rates, with the inhibitory neuron population shadowing activity in the excitatory population. As recurrent excitation increases, as does excitation to the inhibitory neuron population. In response, inhibitory neuron firing increases, feeding inhibition back to the excitatory population. These dynamics are enhanced in the small network as a result of the sparse connectivity; fewer neurons to communicate changes in firing rates slows the dynamic response of

the network. Importantly, reduction in network size does not dramatically alter the Poisson-like characteristics of neuron spike trains, although the network shows a degree of synchronicity in a small subset of excitatory neurons (where  $c_{mn} = 0.1$  to 0.3). In both networks, the strength of individual recurrent excitatory synaptic weights continue to fluctuate while the connection fraction remains stable.

### 4.1.2 LIF-SORN-i

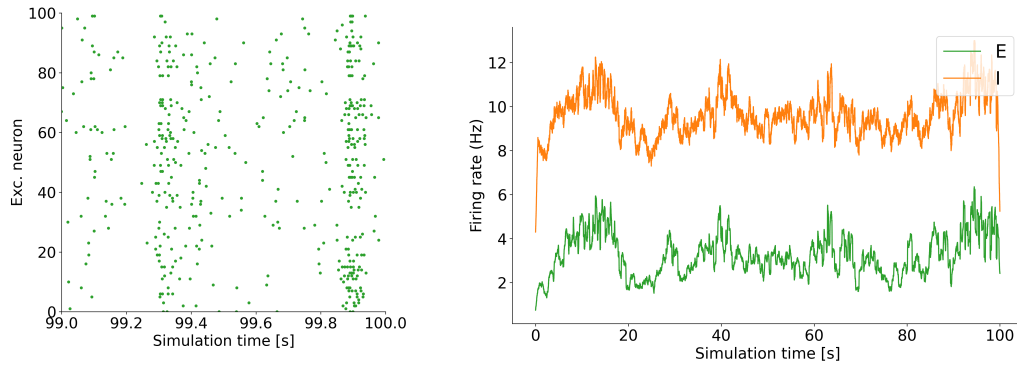


Figure 4.3: LIF-SORN-i excitatory spike trains (left) and population firing rates (right).

The LIF-SORN-i enters into a synchronous firing regime in the absence of external input, shown in Figure 4.3. Firing rates are in accordance with the excitatory target firing rate imposed by intrinsic plasticity. Recurrent excitatory weight dynamics are stable, with rates fluctuating within the midrange of possible values, seen in Figure 4.5.

### 4.1.3 LIF-SORN-c

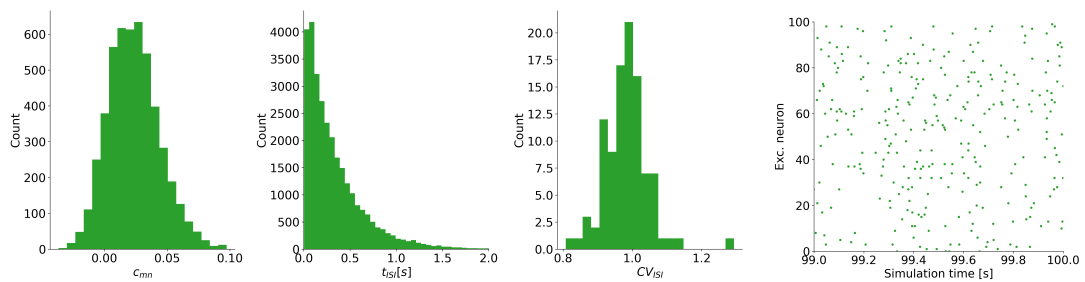


Figure 4.4: LIF-SORN-c excitatory  $c_{mn}$ , ISI, and CV distributions (left) and spike trains (right).

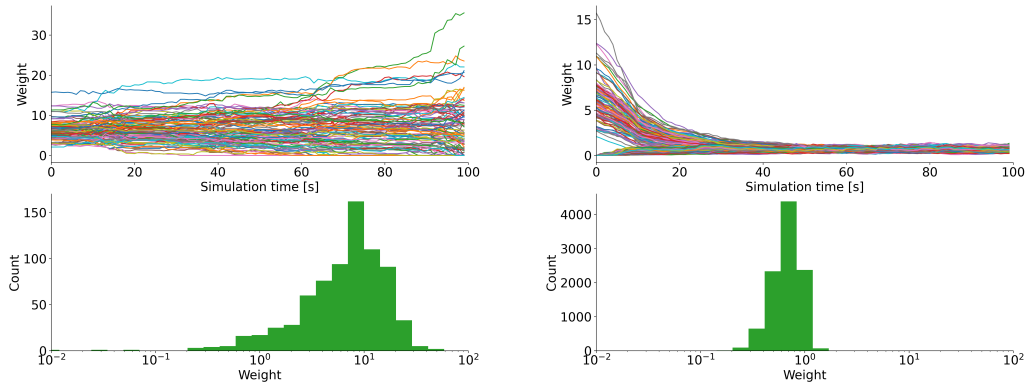


Figure 4.5: Recurrent excitatory weight dynamics (top) and final distributions (bottom) across models. LIF-SORN-i left, LIF-SORN-c right.

The LIF-SORN-c displays prototypical asynchronous, irregular spiking with slowly oscillating average firing rates at low frequencies; coefficient of correlation, interspike interval, and coefficient of variations distributions are akin to those of a Poisson distribution, show in Figure 4.4. Recurrent excitatory synaptic weights converge to a narrow range of values ( $> 2$ ), as seen in Figure 4.5.

## 4.2 Plasticity mechanism knockouts

Miner and Triesch (2016) provide a summary of LIF-SORN network behaviour in the absence of individual plasticity mechanisms, reproduced in Table 4.1.

Mechanism Removal	Result
SN	Weights converge at synaptic maximum or fall below synaptic threshold and are pruned.
IP	Required fine tuning of threshold for stable activity. Failure to tune thresholds leads to silent or “epileptic” networks.
STP	“Epileptic” behaviour leading to structural breakdown.

Table 4.1: Results of plasticity mechanism removal from the LIF-SORN ( $N^E = 1000$ ), recreated from Miner and Triesch (2016).

We investigate how the reduced LIF-SORN variants behave in the absence of the three regulatory mechanisms outlined above. In assessing network stability we examine if it demonstrates a) a relatively constant average firing rate within acceptable biophysical limits, b) steady plastic recurrent excitatory (E) weight dynamics and c)

asynchronous irregular firing. Network behaviour was assessed via population firing rates, neuron spike-trains,  $c_{mn}$ , ISI, and CV distributions, and recurrent E weight dynamics. All plots not provided below are available in Appendix B.

### 4.2.1 LIF-SORN

Results are summarized in Table 4.2.

LIF-SORN	no SN	no IP	no STP
Behaviour	Stationary oscillating firing rates ( $>15$ Hz) after initial peak in activity ( $>20$ Hz). Synchronous spiking in E population ( $c_{mn} = 0$ to $0.8$ ). Super-exponential decay of ISIs. CV distribution heavily right-skewed from 1. Recurrent E weights rapidly diverge toward synaptic weight extrema.	Tapering rapidly fluctuating rates ( $>600$ Hz). Some synchronous firing ( $c_{mn}$ right skewed). Subset of E neurons fire continuously (ISI $\simeq 0$ s). CV distribution centered at 6.5. Erratic E weight dynamics.	Rapid average rates ( $>6000$ Hz) after initial peak ( $>10,000$ Hz). Excessive firing; neurons fire continuously or are silent in E population. All I neurons fire continuously (ISI $\simeq 0$ s). E weights either fixed across simulation or diverge to synaptic extrema.
Conclusions	Network able to maintain low stable firing rates, but compromises asynchronous regime. Behaviour is driven by a population of recurrent excitatory neurons with very strong recurrent connectivity firing in synchrony.	Network displays excessive firing in the absence of IP. Rate behaviour suggests balanced E/I network.	Network is not stable in the absence of STP; strongly epileptic behaviour and breakdown of eTOe weight dynamics.

Table 4.2: Results of plasticity mechanism removal from the LIF-SORN ( $N^E = 100$ ).

### 4.2.2 LIF-SORN-i

Mechanism knockouts are investigated for the LIF-SORN-i with results summarized in Table 4.3.

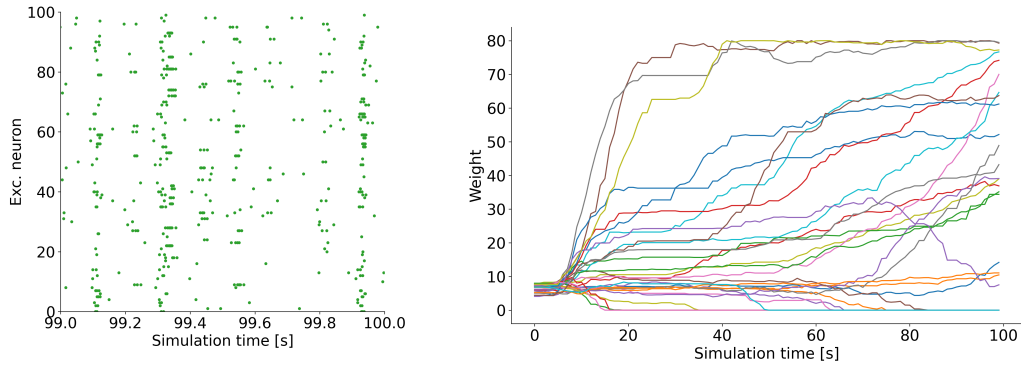


Figure 4.6: LIF-SORN E spike trains (left) and recurrent weights (right) with SN removed.

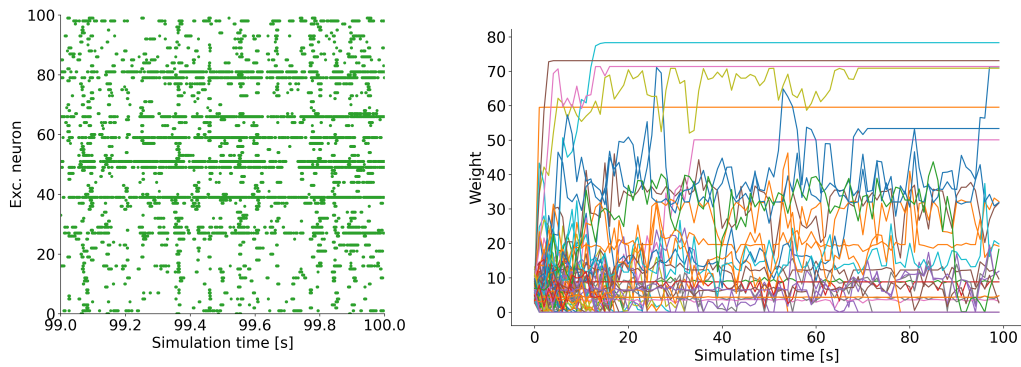


Figure 4.7: LIF-SORN E spike trains (left) and recurrent weights (right) with IP removed.

LIF-SORN-i	no SN	no IP	no STP
Behaviour	Highly synchronous E firing ( $c_{mn} = 0$ to 0.8). Rates approach stationary oscillatory dynamics ( $> 12$ Hz) after initial slow fluctuations ( $> 20$ Hz). E weights grow slowly to synaptic extrema.	Fast oscillating rate averages exponentially decay to $> 200$ Hz. Spike train and $c_{mn}$ do not show synchrony. All neurons fire frequently, subset of E and I neurons fire very rapidly. Some E weights diverge early to extrema.	Initial peak in E firing ( $\approx 10,000$ Hz); drops to silent E network by 40s. I population fires at $\approx 5000$ Hz). Breakdown of E weight dynamics; rapid oscillations followed by constant weights.
Conclusions	Network is stable due to imposed synaptic maximum. Strongly recurrent excitatory network firing in total synchrony.	Network displays stable behaviour at high frequencies.	Network is not stable in absence of STP. Highly epileptic behaviour.

Table 4.3: Results of plasticity mechanism removal from the LIF-SORN-i.

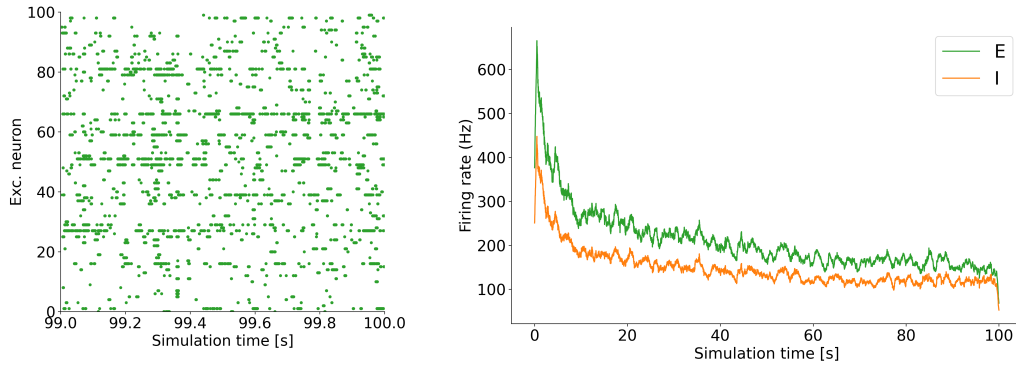


Figure 4.8: LIF-SORN-i E spike trains (left) and population firing rates (right) with IP removed.

### 4.2.3 LIF-SORN-c

Knockout simulations were replicated for the LIF-SORN-c. Results are summarized in Table 4.4.

LIF-SORN-c	no SN	no IP	no STP
Behaviour	Inhibition dominated network; inhibitory neurons fire maximally, excitatory neurons are largely silent. Recurrent E weights show 'staircase' behaviour (weights plateau and then surge in subgroups of population). Surges coincide with small spikes in E activity.	Stationary E and I rates exhibit large-amplitude tightly-coupled oscillations ( $A \simeq 3000$ Hz). Firing asynchronous ( $c_{mn}$ distribution centered at 0.1) yet highly regular (ISIs = 0 to 0.3 s). E weights move in a spastic manner at low values.	Rapid average rates ( $I > 6000$ Hz, $E \simeq 10,000$ Hz). All neurons in network fire continuously (ISI $\simeq 0$ s). Recurrent E weights converge to narrow range of values and do not fluctuate.
Conclusions	Breakdown of network dynamics. Persistent inhibitory activity suggests feedback loop.	Highly active fluctuating regime. Network able to maintain some stability in absence of IP.	Network is unstable in absence of STP; required to limit LTP in recurrent E population and avoid mean-driven regime.

Table 4.4: Results of plasticity mechanism removal from the LIF-SORN-c.

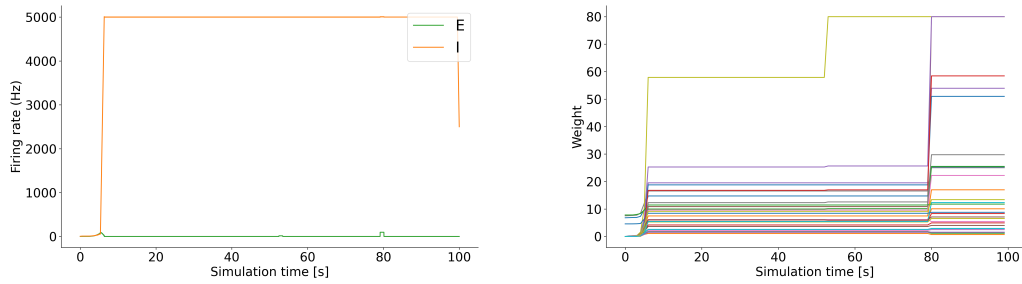


Figure 4.9: LIF-SORN-c population firing rates (left) and recurrent E weights (right) with SN removed.

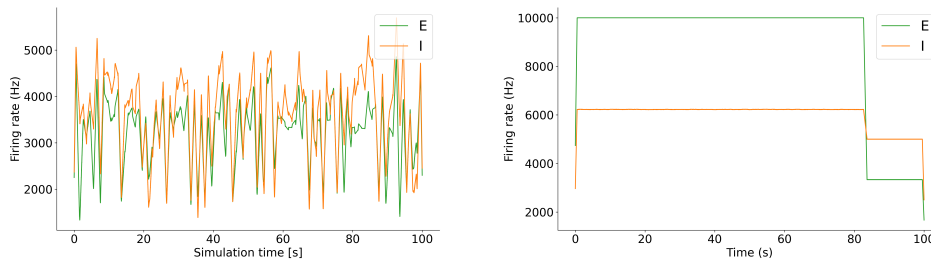


Figure 4.10: LIF-SORN-c population rates in the no IP (left) and no STP (right) conditions.

#### 4.2.4 Discussion

Trace accumulation is responsible for the synchronous behavior observed in the LIF-SORN-i baseline condition, shown in Figure 4.3. The additive nature of the trace updates allows for stronger and more sustained changes in synaptic weights based on spike timing. When multiple presynaptic spikes occur in close proximity to a postsynaptic spike, the accumulated trace values result in larger LTP updates. Strengthening the recurrent synapse further enables spikes in close temporal proximity, increasing LTP and so on. This positive feedback loop reinforces the recurrent firing and promotes synchronization.

The removal of synaptic normalization from the LIF-SORN and LIF-SORN-i is also shown to promote synchrony. Across these models, the removal of SN alters network dynamics but does not compromise overall stability. Neurons fire together at regular intervals while adhering to biophysical constraints, shown in Figure 4.6. The growth of synaptic weights towards their maximum is driven by recurrent excitation. In the absence of SN to maintain a constant total synaptic drive, synaptic weights increase as long as coincident firing occurs. Firing is driven by a subset of excitatory neurons with strong recurrent connections spiking in synchrony. It is important to note that the

networks would likely exhibit epileptic behavior if the artificially imposed minimum and maximum firing rates were removed alongside synaptic normalization.

Across models, the removal of intrinsic plasticity does not significantly increase network synchrony; instead, it broadens the spectrum of firing rates. A small subset of excitatory and inhibitory neurons display elevated firing rates, approximately five times higher than their respective populations, as shown in Figures 4.7 and 4.8. Under baseline conditions, IP caps these firing rates, preventing any single neuron's activity from dominating the network. Without IP, this rate limitation is lifted, leading to increased excitatory firing rates and a rapid rise in a subset of recurrent excitatory weights. Despite these alterations, the population rates continue to fluctuate in near symmetry, with closely matched amplitudes indicating dynamic oscillatory behavior driven by balanced excitation and inhibition, as illustrated in Figure 4.10. The LIF-SORN and LIF-SORN-i networks further demonstrate adaptive capacity, with average population firing rates gradually decaying over time (Figure 4.8), suggesting a progression toward steady-state activity. While some recurrent excitatory weights approach the synaptic maximum (Figure 4.7), the remaining weights fluctuate rapidly, contributing to the network's homeostatic regulation.

The removal of short-term plasticity induces epileptic behaviour in the LIF-SORN and LIF-SORN-c. Neurons fire between 2000 and 10,000 Hz (Figure 4.10), ignoring imposed refractory periods. This suggests that STP exerts a stronger regulatory influence on recurrent excitation than SN or IP. The loss of STP may shift the network to a mean-driven regime, in which the membrane potential resides above spike threshold and drives average network activity, leading to higher firing rates and regular spiking (Petersen & Berg, 2016). This shift is typically associated with an imbalance in E/I activity. As the strongly recurrent excitatory population self-amplifies, the fixed inhibitory population fails to adequately counterbalance the excitatory activity in the absence of STP. Future work could explore introducing plasticity to inhibitory synapses, allowing inhibitory neurons and their targets to sustain co-activity and potentially maintain a fluctuation-driven regime in the absence of STP.

Post hoc analysis revealed that low ( $> 12$  Hz) stationary oscillating rates and asynchronous irregular firing could be artificially restored by reducing the synaptic weight maximum by a factor of 10 to counteract the removal of IP, and by a factor of 100 to counteract the removal of STP. These observations indicate the network might sustain retain baseline stability in the absence of IP and STP under certain parameterizations, however further study is required to make robust conclusions.

Two deviations from the trends described above were observed; both the LIF-SORN-i in the absence of STP, and the LIF-SORN-c in the absence of SN, resulted in a pathologically inhibition-dominated network, where all I neurons fired maximally and E neurons fell silent within the first few seconds of simulation. During this initial period, recurrent excitatory weights display a sharp increase, leading to a rise in the average excitatory firing rate. To mitigate the effects of runaway recurrent excitation, intrinsic plasticity likely causes a substantial increase in the firing threshold of excitatory neurons. Following, recurrent excitatory weights exhibit a ‘staircase’ pattern, characterized by periods of stagnation followed by surges towards the synaptic maximum (see Figure 4.9). These surges occur when spontaneous activity drives E neuron voltage above the elevated threshold set by IP. The increases in E weights correspond to small spikes in E activity, which then drop to 0 Hz due to dominant inhibitory activity. The stagnation of the recurrent weights coincides with the excitatory firing rate falling to zero; once E activity is suppressed, spontaneous activity is not able to initiate firing and the network cannot learn/recover from silence. Meanwhile, the firing rate of the inhibitory population remains unchanged. Despite the expectation that the I population would become inactive without excitatory input, recurrent inhibitory firing may reach postsynaptic membranes at times when the membrane potential is below the inhibitory reversal potential, resulting in a depolarizing (positive) current. This condition can sustain or even enhance neural activity in the absence of excitation. We speculate that the simulations which elicit pathological inhibition introduce a configuration where inhibitory spike arrives at the postsynaptic membrane when the membrane potential is below the reversal potential, eliciting an excitatory effect. As such, both stability and structural integrity are lost.

Finally, the interaction of the voltage-dependent plasticity rule and IP has several interesting implications for network dynamics. In general, it makes the network more ‘sensitive’ to manipulation. This sensitivity can be attributed to mismatch between Hebbian and homeostatic criteria. The LIF-SORN’s intrinsic plasticity mechanism works to maintain a target *firing rate* in excitatory neurons whereas the voltage-dependent learning rule is dependent on the (instantaneous) postsynaptic *membrane potential* to elicit LTP updates. The mismatch in criteria results in opposing effects. For instance, when an excitatory neuron fires above target ( $> 3$  Hz), IP increases its threshold membrane potential in an attempt to limit activity. Subsequently, the neuron’s subthreshold membrane potential increases. The LTP update is proportional to the instantaneous membrane potential. Therefore, when LTP criterion are met, the weight update is exaggerated, and recurrent excitation is facilitated, and IP must increase the spike threshold

and so on.

Furthermore, in all simulations exhibiting stable activity, the recurrent excitatory weights in the LIF-SORN-c were driven down and stabilized at low values (see Figure 4.5). It is likely that the imposed target firing rate is incompatible with the voltage-dependent plasticity rule as at low frequencies. Classic correlation-based learning does not care about membrane potential, updating synaptic weights whenever coincident firing occurs within a specified time-frame. It therefore handles low frequency ranges well. Conversely, voltage-dependence imposes an additional requirement on LTP updates, specifying that the instantaneous post-synaptic membrane must be above a threshold  $\theta_+$ . The network likely experiences silent learning periods, where coincident firing occurs, but does not result in LTP, as average membrane potential does not exceed this threshold. LTD is not gated by such harsh criterion, and drives recurrent excitatory weights down.

### 4.3 Ocular Dominance

The ability to distinguish similar, yet distinct patterns of sensory input is core feature of the nervous system (Cayco-Gajic et al., 2017). To assess if the models could develop meaningful connectivity structure to sensory input, a biologically relevant input paradigm was employed. Ocular dominance (OD) - the differential activation of neurons by visual stimuli to each eye - is a well-documented physiological phenomenon. Empirical studies show retinal waves - brief, high-frequency events propagating from the retina to the primary visual cortex - drive ocular segregation prior to eye-opening (Ackman et al., 2012). Activity is highly correlated within a retina, and decorrelated between retinas. To simulate these conditions, a population of Poisson neurons, separated into two subgroups firing at random alternating intervals, was inputted to the network (Rubisch, 2024). Active input neurons fire at a mean activity of 50 Hz and all remaining non-active neurons fire with background activity of 5 Hz, guaranteeing high correlation within - and limiting correlation between - subgroups, as shown in Figure 4.11.

Excitatory neurons develop ‘preferences’ towards one of the input neuron subgroups by demonstrating differential activation to subgroup firing. Preferences are quantified by the preference score  $D_i$ , which compares the summed strength of all synapses per input subgroup according to

$$D_i = \left( \sum_{j=0}^{0.5N} w_{ij} - \sum_{j=0.5N}^N w_{ij} / \sum_{j=0}^N w_{ij} \right) \quad (4.2)$$

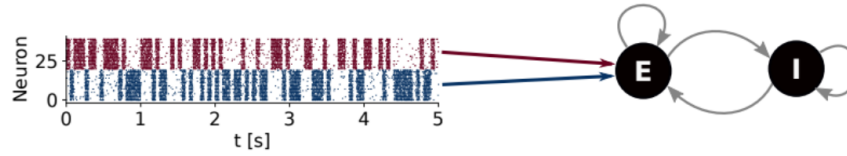


Figure 4.11: Ocular dominance paradigm. Taken with permission from (Rubisch, 2024)

Upon initialization of input synapses, any preferences  $D_i \neq 0$  are caused by random initialization, and synapse connectivity should refine throughout the simulation duration. The feedforward synapse strengths, and preferences score  $D_i$  distributions, were calculated and plotted at regular simulation intervals for each model/mechanism knockout regime, as demonstrated Figure 4.12. Note that synapses connecting input neurons firing in the second subgroup to the E population are negated for distinction in the matrices below.

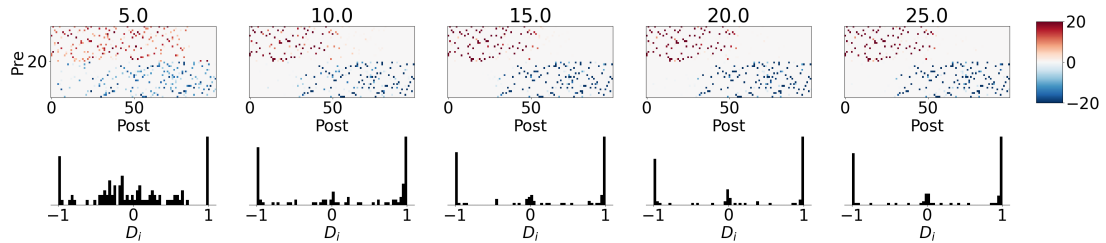


Figure 4.12: Input (pre) to E (post) neuron weights and corresponding preference score distributions over time.

The baseline behaviour of the LIF-SORN, LIF-SORN-i, and LIF-SORN-c are assessed in response to the simulated retinal wave inputs. The networks are initialized and run for 15 seconds to allow the excitatory and inhibitory populations to reach steady-state firing rates before input synapses are established. Since input neurons feed only into the excitatory population, this initially leads to an increase in excitatory activity. The subsequent potentiation of recurrent weights then drives an increase in inhibitory population activity. As the inhibitory influence becomes stronger than the excitatory feed-forward drive, it suppresses the excitatory neurons, resulting in simultaneous peaks in both excitatory and inhibitory activity, as illustrated in Figure 4.13.

### 4.3.1 Baseline performance

Results across model variants are summarized in Table 4.5. All plots not provided in text are available in Appendix C.

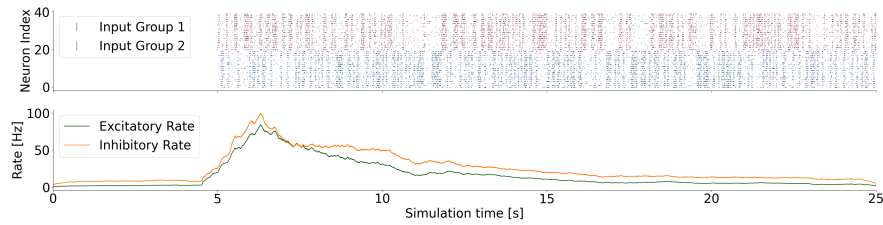


Figure 4.13: Input synapse initialization at  $t = 15$  s, and corresponding E/I rate activity.

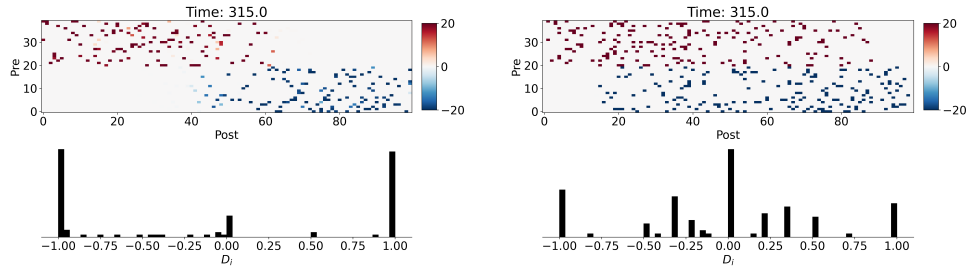


Figure 4.14: Input (pre) to E (post) neuron synapse weights and preference score distributions at simulation endpoint. LIF-SORN (left) and LIF-SORN-c (right).

Model	Behaviour	Conclusions
LIF-SORN	E neurons develop strong preferences ( $D_i \pm 1$ ) to one input subgroup gradually. A small number of preferences converge to $D_i = 0$ . Input weights show distinct segregation between weight extremes early in simulation time. Weak recurrent E activity. Recurrent E weights distributed across moderate values.	LIF-SORN is effective in performing the ocular segregation input task.
LIF-SORN-i	E neurons develop strong preferences ( $D_i \pm 1$ ) to one input subgroup rapidly. A small number of neuron preferences converge to $D_i = 0$ . Input weights show deviate to extrema very early in simulation time. Moderate recurrent E activity.	LIF-SORN-i is effective in performing the ocular segregation input task.
LIF-SORN-c	E neurons develop weak or moderate preference ( $D_i \pm > 0.5$ ) to one input subgroup rapidly, or preferences score converges to $D_i = 0$ . Input weights driven to the synaptic maximum.	LIF-SORN-c is not effective in performing the ocular segregation task under the given parameters.

Table 4.5: Ocular dominance results across model variants.

### 4.3.2 Plasticity mechanism knockouts

The input segregation results of the LIF-SORN, LIF-SORN-i, and LIF-SORN-c networks across mechanism knockouts are summarized in Table 4.6.

Model	no SN	no IP	no STP
LIF-SORN	E neurons develop strong preferences ( $D_i \pm 1$ ) to one input subgroup gradually. Recurrent E activity elevated compared to baseline. Input synapses rapidly deviate to synaptic extremes. Recurrent E weights distributed across wide range of values.	E neurons develop weak or moderate preference ( $D_i \pm > 0.5$ ) to one input subgroup rapidly, or show no preference ( $D_i = 0$ ). Strong current E and I connectivity. Input weights spike immediately to synaptic maximum. E weights are distributed at synaptic maximum at simulation end.	E neurons develop weak or moderate preference ( $D_i \pm > 0.5$ ) to one input subgroup rapidly, or show no preference ( $D_i = 0$ ). E weights oscillate at synaptic maximum before dropping to weak values. Weak recurrent E activity. Input weights immediately deviate to synaptic extremes and stagnate.
LIF-SORN-i	E neurons develop strong preferences ( $D_i \pm 1$ ) to one input subgroup rapidly. Recurrent E activity elevated compared to baseline. Input synapses rapidly deviate to synaptic extremes. Recurrent E weights distributed across wide range of values.	E neurons develop strong preferences ( $D_i \pm 1$ ) to one input subgroup gradually and erratically. Very sparse eTOe connectivity, strong iTOi connectivity. Input and recurrent E weights oscillate between synaptic extrema throughout simulation.	Some evidence of preference development. Input matrices indicate weak feedforward connectivity. Some neurons develop strong preferences while most do not change from initialization preference. Input and E weights oscillate and then stagnate/plateau early in simulation.
LIF-SORN-c	Excitatory neurons develop weak or moderate preference ( $D_i \pm > 0.5$ ) to one input subgroup rapidly, or show no preference ( $D_i = 0$ ). Weights at ( $D_i \pm 1$ ) are initialization artifact. Recurrent E weights highly active, all weights grow to synaptic maximum. Input weights deviate to synaptic extrema.	E neurons favour one input subgroup preferentially and fluctate continuously. Input weights driven to synaptic minimum. E weights driven to synaptic minimum. Weak sparse recurrent E activity, strong recurrent I activity.	E neurons develop weak preference ( $D_i \pm > 0.5$ ), show no preference ( $D_i = 0$ ), or do not change from initialization preference (weights at ( $D_i \pm 1$ ) are initialization artifact). Epileptic recurrent E excitation. Input and recurrent E weights surge to synaptic maximum immediately.

Table 4.6: Ocular dominance results across model variants with plasticity mechanisms removed.

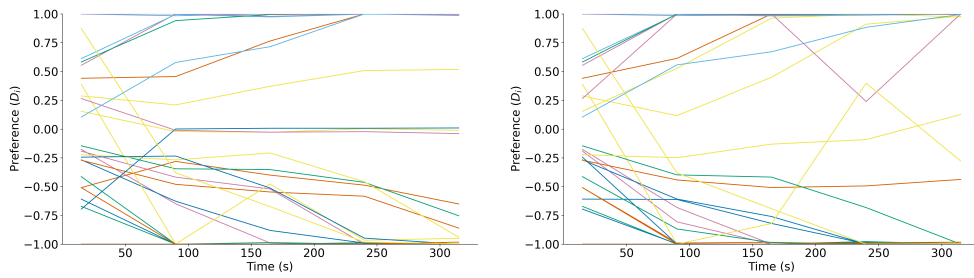


Figure 4.15: E neuron preferences scores over time. LIF-SORN baseline (left) and LIF-SORN with SN removed (right).

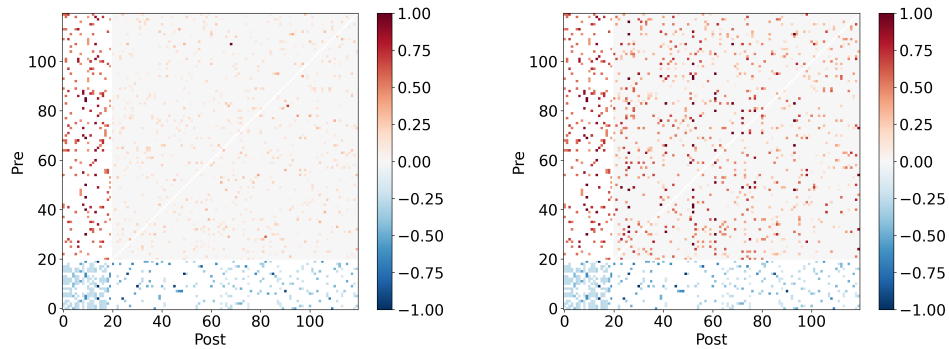


Figure 4.16: Recurrent weight matrices at simulation end. LIF-SORN baseline (left) and LIF-SORN with SN removed (right).

### 4.3.3 Discussion

All models show long-term firing rate stability with the introduction of external input (Figure 4.13). The LIF-SORN and LIF-SORN-i effectively decorrelate inputs in the baseline condition. The behavior of the LIF-SORN-c network is distinct, with poor input decorrelation contrasted to the LIF-SORN in Figure 4.14. It is likely the low-frequency regime, which enforces weak recurrent E weights, impairs the network’s capacity to detect significant correlations in external input. This limitation is evident in both baseline and no-SN ocular dominance conditions, where neurons predominantly exhibit weak preference scores and respond to both input subgroups. When IP is removed, the LIF-SORN-c is shown to develop strong ( $D_i > \pm 0.5$ ) preferences. However, this is not representative of effective input decorrelation as recurrent network activity drives feedforward synapses to  $\simeq 0$ . The preference distribution is an artifact of recurrent network dynamics, rather than a genuine reflection of input decorrelation.

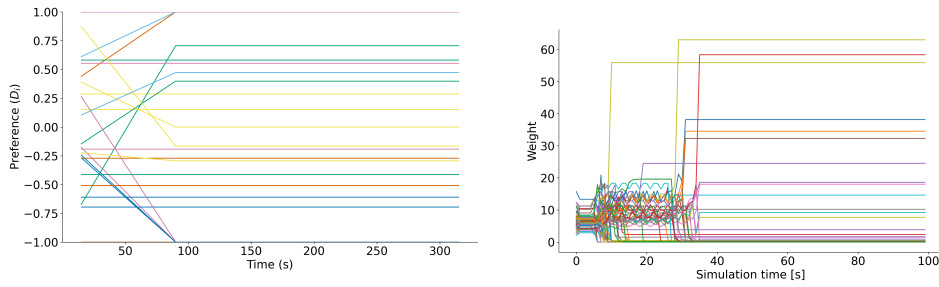


Figure 4.17: LIF-SORN-i preference scores (left) and recurrent weight dynamics (right) with STP removed.

The removal of synaptic normalization is the only HP mechanism knockout in which the LIF-SORN retains the ability to develop strong input segregation. Figure 4.15 plots a random cohort of excitatory neuron preferences over time in the baseline and no-SN conditions, demonstrating that the absence of SN reduces the number of E neurons which equally prefer each input subgroup by the simulation endpoint. The more complete input segregation can be attributed to the increase in recurrent E synchrony known to be induced by the absence of SN. By recruiting neurons into synchronous firing patterns, the network effectively amplifies the signals from the input subgroups. Recurrent E weight dynamics demonstrate elevated synaptic strengthening compared to baseline (Figure 4.16). As a result, neurons which may otherwise avoid segregation are more likely to develop strong connections with particular input subgroups, rather than forming weaker, non-specific connections across multiple groups. This behaviour is also demonstrated across the baseline and no-SN conditions in the LIF-SORN-i network, as well as when comparing the baseline conditions of the LIF-SORN and LIF-SORN-i. An increase in network synchrony driven by runaway recurrent excitation consistently correlates to faster and more complete input segregation. This finding is supported by modelling efforts which show recurrent networks amplify pattern decorrelation in comparison to feedforward networks (Wiechert et al., 2010).

The removal of intrinsic plasticity demonstrates varied effects across models. The LIF-SORN is not able to develop strong input preferences. Rather, preferences scores converge from initialization to  $D_i \pm > 0.5$ , with  $D_i \pm 1$  shown to be an artifact of initialization. Compared to baseline performance, the no-IP condition shows highly active recurrent E and I networks. We also observe from earlier analysis that the removal of IP substantially increases network firing, but does not increase synchrony. It is likely that the very strong recurrent E activity (E firing rates spike to  $>600$  Hz, see Table 4.2), far outweighs the 50 Hz input frequencies. In the absence of excess

synchrony, the network cannot decorrelate feedforward inputs, as network activity is driven by dominant E/I recurrent dynamics. This behaviour is contrasted with the LIF-SORN-i in the absence of IP, wherein some neurons are able to develop strong input preferences. However, neuron preferences are somewhat erratic; after diverging to  $D_i \pm 1$ , neurons may show a reversal in preference, or return to the mid-line. The same explanatory factors apply to the LIF-SORN-i; elevated network synchrony drives input segregation while elevated E and I recurrent dynamics override feedforward inputs. Elevated baseline synchrony gives the LIF-SORN-i a ‘fighting chance’ in the presence of dominant E/I dynamics, where the LIF-SORN has none.

In the absence of STP, none of the networks effectively decorrelate feedforward inputs. STP has been demonstrated to exert the most significant regulatory influence on network behavior, with its removal resulting in excessively high population firing rates, continuous firing, and a disruption in recurrent excitatory synapse dynamics. Among the models, the LIF-SORN-i stands out as the only network demonstrating some degree of input decorrelation in a small subset of excitatory neurons early in the simulation. Correspondingly, a subset of recurrent excitatory and input weights oscillate before stagnating, show in Figure 4.17. The preferences of all other neurons are fixed from initialization. It is probable that the simulated retinal waves initially influence network connectivity before the effects of recurrent activity overshadow their impact.

# Chapter 5

## Conclusions

This paper investigated the interactions between Hebbian and homeostatic plasticity in simulated neural networks. To address complexity within the field, Table 2.1 compiled commonly referenced modeling studies and abstracted pertinent trends. We introduced the reduced LIF-SORN network, and two novel model variants, and investigated how small changes in network composition affect behaviour and stability. The reduced LIF-SORN is shown to preserve network properties characteristic of the original model, maintaining a fluctuation-driven regime. The LIF-SORN-c and LIF-SORN-i networks alter the classical spike-timing dependent plasticity rule by introducing postsynaptic membrane voltage dependence and incremental potentiation and depression trace updates, respectively. The networks were comparatively assessed through the systematic knockout of the synaptic normalization, intrinsic plasticity, and short-term plasticity homeostatic mechanisms in response to spontaneous and input-driven firing.

Several themes can be drawn from this experimental work. Under the simulated parameters, synaptic normalization is often necessary to maintain asynchronous firing but not network stability. Intrinsic plasticity is necessary to limit runaway firing and network regularity, and indirectly facilitates firing asynchrony. Short-term plasticity is often both necessary and sufficient to maintain valid recurrent excitatory dynamics. However, stability could be enforced by placing strict maximum weight values on the recurrent excitatory synapses. Sweeps through parameter space are a necessary direction of future work to make robust generalized claims about network stability under these manipulations.

The interplay between voltage-dependent LTP and the variable excitatory spiking threshold makes the LIF-SORN-c network's learning dynamics more context-sensitive and variable than its voltage-independent counterparts. In low-frequency regimes,

LTD dominates over LTP, driving recurrent excitatory weights down and limiting the network's ability to learn effectively in response to external inputs. The original paper from Clopath et al. (2010) employs homogeneous Hebbian and homeostatic plasticity mechanisms, with the neuron model directly controlling membrane potential statistics. This approach likely eases parameter tuning, and avoids entering into parameter spaces where the mechanisms amplify each other's effects to the detriment of model stability, as seen in the heterogeneous approach investigated above. This further serves to demonstrate the importance of selecting appropriate homeostatic balance parameters in investigating spiking network dynamics.

The LIF-SORN and LIF-SORN-c networks lie in asynchronous irregular fluctuation-driven regimes in the absence of induced activity. The addition of cumulative trace updates introduced the potential for feedback loops in network learning. In amplifying LTP, the LIF-SORN-i demonstrates spontaneous synchrony. While this synchrony was shown to have a 'protective' effect on input segregation efficacy, this STDP mechanism may not be biologically valid. Empirical work by Froemke and Dan (2002) demonstrates that, while synaptic modification depends on the timing of preceding spikes beyond the interval of the most recent spike pair, the efficacy of each spike in synaptic modification is *suppressed* by spikes in the same neuron in recent history. This non-linearity is effectively captured by triplet learning rules, which use three spikes (triplets) instead of pairs to induce potentiation. While the voltage-dependent learning rule employed above does account for the effects of previous spikes upon the weight change induced by the most recent spike pair, in future work we recommend simulating a simple triplet-spiking model, to differentiate the impact of voltage-dependence and non-linear trace effects. Gjorgjieva et al. (2011) presents a promising candidate for such an investigation.

Finally, decorrelation is a fundamental strategy to improve neural codes, aiming to reduce redundancies and distribute neuronal activity patterns more evenly over coding space to extract small differences from overlapping sensory inputs. How recurrent spiking neural networks achieve input decorrelation remains an open question in the field (Wiechert et al., 2010). Principle component analysis (PCA)-like strategies are sufficient for capturing data structures in which linear pairwise correlations are the most important form of statistical dependence, such as in the ocular dominance task simulated above. However, natural stimuli contain higher-order data structures which are not well captured by orthogonal components. For instance, lines and edges cannot be characterized by linear pairwise statistics (Olshausen & Field, 1996).

In presenting the network with non-linearly separable source factors, such as in the

stripes-and-bars problem (Foldiak, 2002), the network would need to extract independent factors from higher-dimensional data, akin to independent component analysis (ICA)-like strategies. Exploring the minimal set of learning rules required to achieve ICA-like encoding of natural stimuli is a valuable avenue for future research. Although the challenge of understanding how plasticity rules can implement ICA-like strategies remains, Savin et al. (2010) propose a promising candidate model that involves interactions between STDP, IP, and SN.

# Bibliography

- Abbott, L. F., Varela, J. A., Sen, K., & Nelson, S. B. (1997). Synaptic Depression and Cortical Gain Control. *Science*, *275*(5297), 221–224. <https://doi.org/10.1126/science.275.5297.221>
- Abbott, L. F., & Dayan, P. (2001). *Theoretical neuroscience*. The MIT Press.
- Ackman, J. B., Burbridge, T. J., & Crair, M. C. (2012). Retinal waves coordinate patterned activity throughout the developing visual system. *Nature*, *490*(7419), 219–225. <https://doi.org/10.1038/nature11529>
- Artola, A., Bröcher, S., & Singer, W. (1990). Different voltage-dependent thresholds for inducing long-term depression and long-term potentiation in slices of rat visual cortex. *Nature*, *347*(6288), 69–72. <https://doi.org/10.1038/347069a0>
- Benuskova, L., & Abraham, W. C. (2007). STDP rule endowed with the BCM sliding threshold accounts for hippocampal heterosynaptic plasticity. *Journal of Computational Neuroscience*, *22*(2), 129–133. <https://doi.org/10.1007/s10827-006-0002-x>
- Bienenstock, E., Cooper, L., & Munro, P. (1982). Theory for the development of neuron selectivity: Orientation specificity and binocular interaction in visual cortex. *The Journal of Neuroscience*, *2*(1), 32–48. <https://doi.org/10.1523/JNEUROSCI.02-01-00032.1982>
- Bosch, M., Castro, J., Saneyoshi, T., Matsuno, H., Sur, M., & Hayashi, Y. (2014). Structural and Molecular Remodeling of Dendritic Spine Substructures during Long-Term Potentiation. *Neuron*, *82*(2), 444–459. <https://doi.org/10.1016/j.neuron.2014.03.021>
- Bourne, J. N., & Harris, K. M. (2011). Coordination of size and number of excitatory and inhibitory synapses results in a balanced structural plasticity along mature hippocampal ca1 dendrites during ltp. *Hippocampus*, *21*(4), 354. <https://doi.org/10.1002/hipo.20768>

- Bredenberg, C., & Savin, C. (2023). Desiderata for normative models of synaptic plasticity. *ArXiv*. Retrieved August 6, 2024, from <https://www.semanticscholar.org/paper/63fb1f87f2d1c64dee3974cbcdcb52ffef49a9b8>
- Brian2. (2024). *Brian 2 documentation* [Accessed: 2024-08-29]. <https://brian2.readthedocs.io/en/2.7.1/>
- Burrone, J., O’Byrne, M., & Murthy, V. N. (2002). Multiple forms of synaptic plasticity triggered by selective suppression of activity in individual neurons. *Nature*, *420*(6914), 414–418. <https://doi.org/10.1038/nature01242>
- Cayco-Gajic, N. A., Clopath, C., & Silver, R. A. (2017). Sparse synaptic connectivity is required for decorrelation and pattern separation in feedforward networks. *Nature Communications*, *8*(1), 1116. <https://doi.org/10.1038/s41467-017-01109-y>
- Chen, J.-Y., Lonjers, P., Lee, C., Chistiakova, M., Volgushev, M., & Bazhenov, M. (2013). Heterosynaptic Plasticity Prevents Runaway Synaptic Dynamics. *The Journal of Neuroscience*, *33*(40), 15915–15929. <https://doi.org/10.1523/JNEUROSCI.5088-12.2013>
- Clopath, C., Büsing, L., Vasilaki, E., & Gerstner, W. (2010). Connectivity reflects coding: A model of voltage-based STDP with homeostasis. *Nature Neuroscience*, *13*(3), 344–352. <https://doi.org/10.1038/nn.2479>
- Cooper, L. N., & Bear, M. F. (2012). The BCM theory of synapse modification at 30: Interaction of theory with experiment. *Nature Reviews. Neuroscience*, *13*(11), 798–810. <https://doi.org/10.1038/nrn3353>
- Cooper, L. N., Intrator, N., Blais, B. S., & Shouval, H. Z. (2004). Theory of Cortical Plasticity. <https://doi.org/10.1142/5462>
- Davis, G. W., & Bezprozvanny, I. (2001). Maintaining the stability of neural function: A homeostatic hypothesis. *Annual Review of Physiology*, *63*, 847–869. <https://doi.org/10.1146/annurev.physiol.63.1.847>
- Davis, G. W. (2013). Homeostatic signaling and the stabilization of neural function. *Neuron*, *80*(3), 718–728. <https://doi.org/10.1016/j.neuron.2013.09.044>
- Desai, N. S. (2003). Homeostatic plasticity in the CNS: Synaptic and intrinsic forms. *Journal of Physiology-Paris*, *97*(4), 391–402. <https://doi.org/10.1016/j.jphysparis.2004.01.005>
- Desai, N. S., Cudmore, R. H., Nelson, S. B., & Turrigiano, G. G. (2002). Critical periods for experience-dependent synaptic scaling in visual cortex. *Nature Neuroscience*, *5*(8), 783–789. <https://doi.org/10.1038/nn878>

- Elliott, T., & Shadbolt, N. R. (2002). Multiplicative synaptic normalization and a nonlinear Hebb rule underlie a neurotrophic model of competitive synaptic plasticity. *Neural Computation*, *14*(6), 1311–1322. <https://doi.org/10.1162/089976602753712954>
- Finelli, L. A., Haney, S., Bazhenov, M., Stopfer, M., & Sejnowski, T. J. (2008). Synaptic Learning Rules and Sparse Coding in a Model Sensory System. *PLoS Computational Biology*, *4*(4), e1000062. <https://doi.org/10.1371/journal.pcbi.1000062>
- Foldiak, P. (2002). Sparse coding in the primate cortex. *The Handbook of Brain Theory and Neural Networks*, *2*.
- Fong, M.-f., Newman, J. P., Potter, S. M., & Wenner, P. (2015). Upward synaptic scaling is dependent on neurotransmission rather than spiking. *Nature Communications*, *6*, 6339. <https://doi.org/10.1038/ncomms7339>
- Fox, K., & Stryker, M. (2017). Integrating Hebbian and homeostatic plasticity: Introduction. *Philosophical Transactions of the Royal Society B: Biological Sciences*, *372*(1715), 20160413. <https://doi.org/10.1098/rstb.2016.0413>
- Froemke, R. C., & Dan, Y. (2002). Spike-timing-dependent synaptic modification induced by natural spike trains. *Nature*, *416*(6879), 433–438. <https://doi.org/10.1038/416433a>
- Gainey, M. A., & Feldman, D. E. (2017). Multiple shared mechanisms for homeostatic plasticity in rodent somatosensory and visual cortex. *Philosophical Transactions of the Royal Society B: Biological Sciences*, *372*(1715), 20160157. <https://doi.org/10.1098/rstb.2016.0157>
- Gerstner, W., & Kistler, W. M. (2002). Mathematical formulations of Hebbian learning. *Biological Cybernetics*, *87*(5), 404–415. <https://doi.org/10.1007/s00422-002-0353-y>
- Gjorgjieva, J., Clopath, C., Audet, J., & Pfister, J.-P. (2011). A triplet spike-timing-dependent plasticity model generalizes the Bienenstock–Cooper–Munro rule to higher-order spatiotemporal correlations. *Proceedings of the National Academy of Sciences*, *108*(48), 19383–19388. <https://doi.org/10.1073/pnas.1105933108>
- Hebb, D. O. (1949, May). *The Organization of Behavior: A Neuropsychological Theory*. Psychology Press. <https://doi.org/10.4324/9781410612403>
- Hengen, K. B., Lambo, M. E., Van Hooser, S. D., Katz, D. B., & Turrigiano, G. G. (2013). Firing Rate Homeostasis in Visual Cortex of Freely Behaving Rodents. *Neuron*, *80*(2), 10.1016/j.neuron.2013.08.038. <https://doi.org/10.1016/j.neuron.2013.08.038>

- Hennig, M. H., Grady, J., Copenhagen, J. v., & Sernagor, E. (2011). Age-dependent Homeostatic Plasticity of GABAergic Signaling in Developing Retinal Networks [Publisher: Society for Neuroscience Section: Brief Communications]. *Journal of Neuroscience*, *31*(34), 12159–12164. <https://doi.org/10.1523/JNEUROSCI.3112-11.2011>
- Keck, T., Toyozumi, T., Chen, L., Doiron, B., Feldman, D. E., Fox, K., Gerstner, W., Haydon, P. G., Hübener, M., Lee, H.-K., Lisman, J. E., Rose, T., Sengpiel, F., Stellwagen, D., Stryker, M. P., Turrigiano, G. G., & van Rossum, M. C. (2017). Integrating Hebbian and homeostatic plasticity: The current state of the field and future research directions. *Philosophical Transactions of the Royal Society B: Biological Sciences*, *372*(1715), 20160158. <https://doi.org/10.1098/rstb.2016.0158>
- Kempler, R., Gerstner, W., & van Hemmen, J. L. (1999). Hebbian learning and spiking neurons. *Physical Review E*, *59*(4), 4498–4514. <https://doi.org/10.1103/PhysRevE.59.4498>
- Kirkwood, A., Rioult, M. G., & Bear, M. F. (1996). Experience-dependent modification of synaptic plasticity in visual cortex. *Nature*, *381*(6582), 526–528. <https://doi.org/10.1038/381526a0>
- Klos, C., Miner, D., & Triesch, J. (2018). Bridging structure and function: A model of sequence learning and prediction in primary visual cortex. *PLOS Computational Biology*, *14*(6), e1006187. <https://doi.org/10.1371/journal.pcbi.1006187>
- Koulakov, A. A., Hromádka, T., & Zador, A. M. (2009). Correlated connectivity and the distribution of firing rates in the neocortex. *The Journal of Neuroscience: The Official Journal of the Society for Neuroscience*, *29*(12), 3685–3694. <https://doi.org/10.1523/JNEUROSCI.4500-08.2009>
- Lazar, A., Pipa, G., & Triesch, J. (2009). SORN: A self-organizing recurrent neural network. *Frontiers in Computational Neuroscience*, *3*. <https://doi.org/10.3389/neuro.10.023.2009>
- Lisman, J., & Spruston, N. (2005). Postsynaptic depolarization requirements for LTP and LTD: A critique of spike timing-dependent plasticity. *Nature Neuroscience*, *8*(7), 839–841. <https://doi.org/10.1038/nn0705-839>
- Litwin-Kumar, A., & Doiron, B. (2014). Formation and maintenance of neuronal assemblies through synaptic plasticity. *Nature Communications*, *5*(1), 5319. <https://doi.org/10.1038/ncomms6319>

- Loewenstein, Y., Kuras, A., & Rumpel, S. (2011). Multiplicative Dynamics Underlie the Emergence of the Log-Normal Distribution of Spine Sizes in the Neocortex In Vivo. *The Journal of Neuroscience*, *31*(26), 9481–9488. <https://doi.org/10.1523/JNEUROSCI.6130-10.2011>
- Miller, K. D., & MacKay, D. J. C. (1994). The Role of Constraints in Hebbian Learning. *Neural Computation*, *6*(1), 100–126. <https://doi.org/10.1162/neco.1994.6.1.100>
- Miner, D., & Triesch, J. (2016). Plasticity-Driven Self-Organization under Topological Constraints Accounts for Non-random Features of Cortical Synaptic Wiring. *PLOS Computational Biology*, *12*(2), e1004759. <https://doi.org/10.1371/journal.pcbi.1004759>
- Mongillo, G., Rumpel, S., & Loewenstein, Y. (2018). Inhibitory connectivity defines the realm of excitatory plasticity. *Nature Neuroscience*, *21*(10), 1463–1470. <https://doi.org/10.1038/s41593-018-0226-x>
- O’Leary, T., & Wyllie, D. J. A. (2011). Neuronal homeostasis: Time for a change? *The Journal of Physiology*, *589*(20), 4811–4826. <https://doi.org/10.1113/jphysiol.2011.210179>
- Olshausen, B. A., & Field, D. J. (1996). Emergence of simple-cell receptive field properties by learning a sparse code for natural images. *Nature*, *381*(6583), 607–609. <https://doi.org/10.1038/381607a0>
- Papa, B. D., Priesemann, V., & Triesch, J. (2017). Criticality meets learning: Criticality signatures in a self-organizing recurrent neural network. *PLOS ONE*, *12*(5), e0178683. <https://doi.org/10.1371/journal.pone.0178683>
- Petersen, P. C., & Berg, R. W. (2016). Lognormal firing rate distribution reveals prominent fluctuation–driven regime in spinal motor networks (J.-M. Ramirez, Ed.). *eLife*, *5*. <https://doi.org/10.7554/eLife.18805>
- Pfister, J.-P., & Gerstner, W. (2006). Triplets of Spikes in a Model of Spike Timing-Dependent Plasticity. *Journal of Neuroscience*, *26*(38), 9673–9682. <https://doi.org/10.1523/JNEUROSCI.1425-06.2006>
- Rubisch, P. (2024). The interplay between voltage-dependent plasticity, inhibition and network structure in spiking neuronal network models.
- Savin, C., Joshi, P., & Triesch, J. (2010). Independent Component Analysis in Spiking Neurons. *PLoS Computational Biology*, *6*(4), e1000757. <https://doi.org/10.1371/journal.pcbi.1000757>
- Shouval, H. Z., Bear, M. F., & Cooper, L. N. (2002). A unified model of NMDA receptor-dependent bidirectional synaptic plasticity. *Proceedings of the National*

- Academy of Sciences*, 99(16), 10831–10836. <https://doi.org/10.1073/pnas.152343099>
- Song, S., Sjöström, P. J., Reigl, M., Nelson, S., & Chklovskii, D. B. (2005). Highly Nonrandom Features of Synaptic Connectivity in Local Cortical Circuits. *PLOS Biology*, 3(3), e68. <https://doi.org/10.1371/journal.pbio.0030068>
- Soures, N., Hays, L., Bohannon, E., Ziyarah, A. M., & Kudithipudi, D. (2017). On-device STDP and synaptic normalization for neuromemristive spiking neural network [ISSN: 1558-3899]. *2017 IEEE 60th International Midwest Symposium on Circuits and Systems (MWSCAS)*, 1081–1084. <https://doi.org/10.1109/MWSCAS.2017.8053115>
- Suratkal, S. S., Yen, Y.-H., & Nishiyama, J. (2021). Imaging dendritic spines: Molecular organization and signaling for plasticity. *Current Opinion in Neurobiology*, 67, 66–74. <https://doi.org/10.1016/j.conb.2020.08.006>
- Sweeney, Y., Kotaleski, J. H., & Hennig, M. H. (2015). A Diffusive Homeostatic Signal Maintains Neural Heterogeneity and Responsiveness in Cortical Networks. *PLOS Computational Biology*, 11(7), e1004389. <https://doi.org/10.1371/journal.pcbi.1004389>
- Tetzlaff, C., Kolodziejcki, C., Timme, M., & Wörgötter, F. (2011). Synaptic scaling in combination with many generic plasticity mechanisms stabilizes circuit connectivity. *Frontiers in Computational Neuroscience*, 5, 47. <https://doi.org/10.3389/fncom.2011.00047>
- Thomson, A. M., West, D. C., Wang, Y., & Bannister, A. P. (2002). Synaptic connections and small circuits involving excitatory and inhibitory neurons in layers 2–5 of adult rat and cat neocortex: Triple intracellular recordings and biocytin labelling in vitro. *Cerebral Cortex*, 12(9), 936–953. <https://doi.org/10.1093/cercor/12.9.936>
- Toyoizumi, T., Kaneko, M., Stryker, M. P., & Miller, K. D. (2014). Modeling the dynamic interaction of Hebbian and homeostatic plasticity. *Neuron*, 84(2), 497–510. <https://doi.org/10.1016/j.neuron.2014.09.036>
- Toyoizumi, T., Miyamoto, H., Yazaki-Sugiyama, Y., Atapour, N., Hensch, T. K., & Miller, K. D. (2013). A Theory of the Transition to Critical Period Plasticity: Inhibition Selectively Suppresses Spontaneous Activity. *Neuron*, 80(1), 51–63. <https://doi.org/10.1016/j.neuron.2013.07.022>

- Turrigiano, G. G., Leslie, K. R., Desai, N. S., Rutherford, L. C., & Nelson, S. B. (1998). Activity-dependent scaling of quantal amplitude in neocortical neurons. *Nature*, *391*(6670), 892–896. <https://doi.org/10.1038/36103>
- Turrigiano, G. G. (1999). Homeostatic plasticity in neuronal networks: The more things change, the more they stay the same. *Trends in Neurosciences*, *22*(5), 221–227. [https://doi.org/10.1016/S0166-2236\(98\)01341-1](https://doi.org/10.1016/S0166-2236(98)01341-1)
- Turrigiano, G. G. (2017). The dialectic of Hebb and homeostasis. *Philosophical Transactions of the Royal Society B: Biological Sciences*, *372*(1715), 20160258. <https://doi.org/10.1098/rstb.2016.0258>
- von der Malsburg, C. (1973). Self-organization of orientation sensitive cells in the striate cortex. *Kybernetik*, *14*(2), 85–100. <https://doi.org/10.1007/BF00288907>
- Wiechert, M. T., Judkewitz, B., Riecke, H., & Friedrich, R. W. (2010). Mechanisms of pattern decorrelation by recurrent neuronal circuits. *Nature Neuroscience*, *13*(8), 1003–1010. <https://doi.org/10.1038/nn.2591>
- Wilson, H. R., & Cowan, J. D. (1972). Excitatory and inhibitory interactions in localized populations of model neurons. *Biophysical Journal*, *12*(1), 1–24. [https://doi.org/10.1016/S0006-3495\(72\)86068-5](https://doi.org/10.1016/S0006-3495(72)86068-5)
- Wu, Z., & Yamaguchi, Y. (2006). Conserving total synaptic weight ensures one-trial sequence learning of place fields in the hippocampus. *Neural Networks: The Official Journal of the International Neural Network Society*, *19*(5), 547–563. <https://doi.org/10.1016/j.neunet.2005.06.048>
- Xu, M., Liu, F., Hu, Y., Li, H., Wei, Y., Zhong, S., Pei, J., & Deng, L. (2024). Adaptive Synaptic Scaling in Spiking Networks for Continual Learning and Enhanced Robustness. *IEEE transactions on neural networks and learning systems*, *PP*. <https://doi.org/10.1109/TNNLS.2024.3373599>
- Zenke, F., Hennequin, G., & Gerstner, W. (2013). Synaptic Plasticity in Neural Networks Needs Homeostasis with a Fast Rate Detector. *PLOS Computational Biology*, *9*(11), e1003330. <https://doi.org/10.1371/journal.pcbi.1003330>
- Zhang, Y., Behrens, M. M., & Lisman, J. E. (2008). Prolonged Exposure to NMDAR Antagonist Suppresses Inhibitory Synaptic Transmission in Prefrontal Cortex. *Journal of Neurophysiology*, *100*(2), 959–965. <https://doi.org/10.1152/jn.00079.2008>

# Appendix A

## Modelling Parameters

Parameter	Value	Description
<b>Base Parameters</b>		
length_T	2500 $\mu\text{m}$	Sheet length
height_T	1000 $\mu\text{m}$	Sheet height
size_T	[2500, 1000] $\mu\text{m}$	Sheet size
N_e	100	Excitatory population size
N_i	0.2 * N_e	Inhibitory population size
<b>Neuron Parameters</b>		
$\sigma_{noise}$	16 mV	Noise amplitude
$\tau$	20 ms	Membrane time constant
V_r.e	-70 mV	Excitatory reset potential
V_r.i	-60 mV	Inhibitory reset potential
E_l	-60 mV	Resting potential
V_t.i	30 mV	Minus maximum initial threshold voltage
V_t.var	5 mV	Maximum initial threshold voltage swing
V_v.i	50 mV	Minus maximum initial voltage
V_v.var	20 mV	Maximum initial voltage swing
V_v.i.i	50 mV	Minus maximum initial inhibitory voltage
V_v.var.i	20 mV	Maximum initial inhibitory voltage swing
V_t.i	-48 mV	Threshold of inhibitory neurons
<b>Synapse Parameters</b>		
width_T	200 $\mu\text{m}$	Growth radius
sparse_eTOe	0.1	Target recurrent excitatory sparseness
sparse_iTOe	0.1	Inhibitory to excitatory sparseness
sparse_eTOi	0.1	Excitatory to inhibitory sparseness
sparse_iTOi	0.5	Inhibitory to inhibitory sparseness
wi_eTOe	8	Target e $\rightarrow$ e weight
wi_eTOi	1.5	Initial e $\rightarrow$ i weight

Parameter	Value	Description
$w_{i \rightarrow e}^{TOe}$	4	Initial $i \rightarrow e$ weight
$w_{i \rightarrow i}^{TOi}$	4	Initial $i \rightarrow i$ weight
$\text{delay}_{e \rightarrow e}^{TOe}$	3 ms	$e \rightarrow e$ latency
$\text{delay}_{e \rightarrow i}^{TOi}$	1 ms	$e \rightarrow i$ latency
$\text{delay}_{i \rightarrow e}^{TOe}$	2 ms	$i \rightarrow e$ latency
$\text{delay}_{i \rightarrow i}^{TOi}$	2 ms	$i \rightarrow i$ latency
$\tau_e$	3 ms	EPSP time constant
$\tau_i$	5 ms	IPSP time constant
$E_e$	0 mV	Reversal potential for excitation
$E_i$	-80 mV	Reversal potential for inhibition
<b>STDP Parameters</b>		
$\tau_{pre}$	15 ms	Pre-before-post STDP time constant
$\tau_{post}$	30 ms	Post-before-pre STDP time constant
$A_p$	0.48	Potentiating STDP learning rate
$A_d$	-0.24	Depressing STDP learning rate
<b>STP Parameters</b>		
$U$	0.04	Facilitation increment
$\tau_f$	2000 ms	Facilitation time constant
$\tau_d$	500 ms	Depression time constant
<b>Intrinsic Plasticity Parameters</b>		
$h_{ip}$	3 Hz	Target rate
$\eta_{ip}$	0.1 mV	IP learning rate
<b>Synaptic Normalization Parameters</b>		
$\text{total\_in\_eTOe}$	$N_e * \text{sparse\_eTOe} * w_{i \rightarrow e}^{TOe}$	Total $e \rightarrow e$ synaptic input
$\text{total\_in\_iTOe}$	$N_i * \text{sparse\_iTOe} * w_{i \rightarrow e}^{TOe}$	Total $i \rightarrow e$ synaptic input
$\text{total\_in\_eTOi}$	$N_e * \text{sparse\_eTOi} * w_{i \rightarrow e}^{TOi}$	Total $e \rightarrow i$ synaptic input
$\text{total\_in\_iTOi}$	$N_i * \text{sparse\_iTOi} * w_{i \rightarrow i}^{TOi}$	Total $i \rightarrow i$ synaptic input
<b>Structural Plasticity Parameters</b>		
$sp_{initial}$	$1e-2$	Initial weight for newly created synapses
$\text{zero\_cut}$	$1e-3$	Zero pruning cutoff
$\text{sp\_rate}$	6000	Stochastic rate of new synapse production
<b>Clopath STDP Parameters</b>		
$g$	0.067	Gain parameter
$\tau_s$	15 ms	Synaptic time constant
$\tau_m$	10 ms	Membrane time constant
$\tau_p$	7 ms	Potential time constant
$A_d$	0.01	Depression rate

<b>Parameter</b>	<b>Value</b>	<b>Description</b>
$A_p$	0.0002	Potential rate
$\theta_m$	-75 mV	Depression threshold voltage
$\theta_p$	-68 mV	Potential threshold voltage
$\eta$	1	Learning rate
$\tau_w$	1 ms	Time constant for synaptic weight changes
$LTP_{mod}$	1	Long-Term Potentiation modulation
$LTD_{mod}$	1	Long-Term Depression modulation
$min_w$	0	Minimum synaptic weight
$max_w$	total_in_eTOe	Maximum synaptic weight

# Appendix B

## Spontaneous network behaviour

### B.1 Baseline

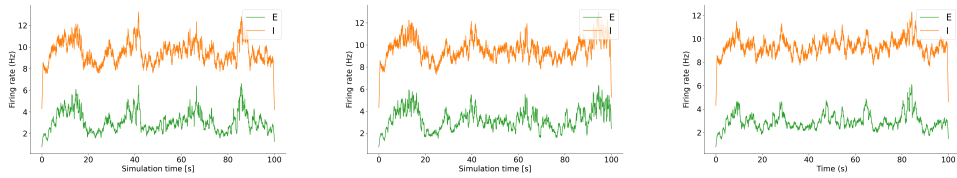


Figure B.1: Baseline population firing rates. LIF-SORN left, LIF-SORN-i center, LIF-SORN-c right.

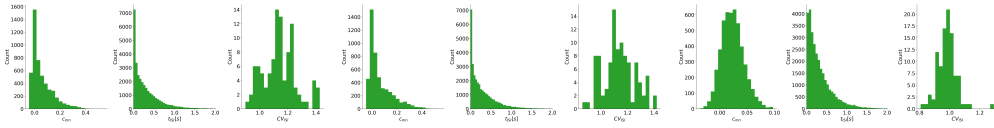


Figure B.2: Baseline  $c_{mn}$ , ISI, and CV distributions. LIF-SORN left, LIF-SORN-i center, LIF-SORN-c right.

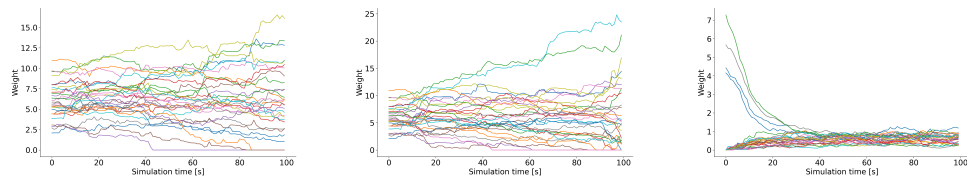


Figure B.3: Baseline recurrent excitatory weight dynamics. LIF-SORN left, LIF-SORN-i center, LIF-SORN-c right.

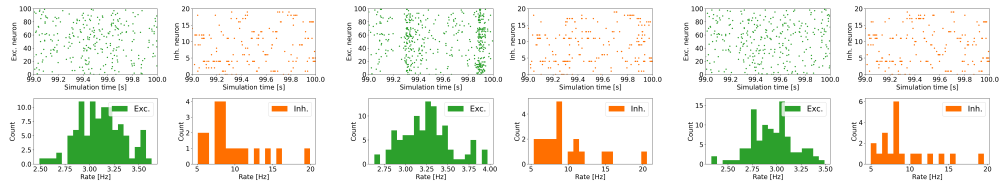


Figure B.4: Baseline E/I spike trains and firing rate distributions. LIF-SORN left, LIF-SORN-i center, LIF-SORN-c right

## B.2 No synaptic normalization

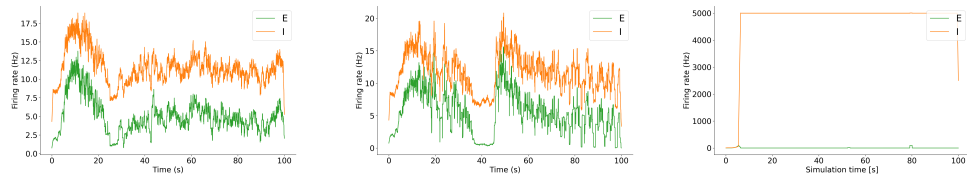


Figure B.5: Population firing rates with SN removed. LIF-SORN left, LIF-SORN-i center, LIF-SORN-c right.

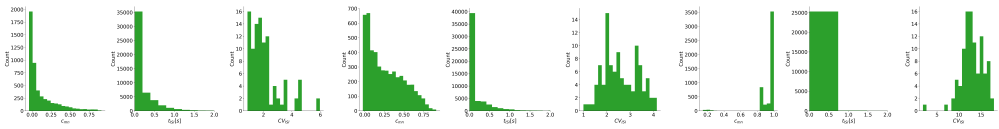


Figure B.6:  $c_{mn}$ , ISI, and CV distributions with SN removed. LIF-SORN left, LIF-SORN-i center, LIF-SORN-c right.

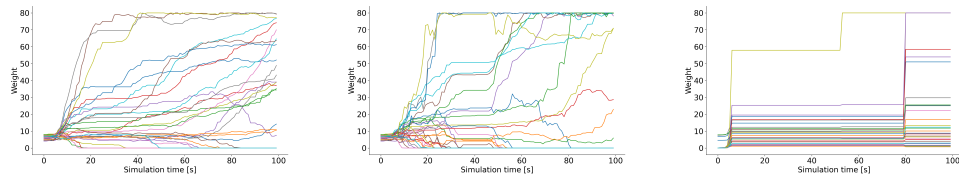


Figure B.7: Recurrent excitatory weight dynamics with SN removed. LIF-SORN left, LIF-SORN-i center, LIF-SORN-c right.

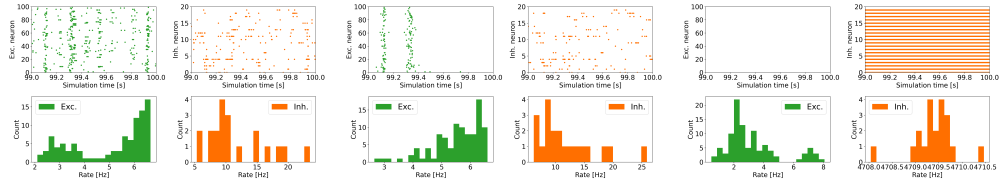


Figure B.8: E/I spike trains and firing rate distributions with SN removed. LIF-SORN left, LIF-SORN-i center, LIF-SORN-c right

### B.3 No intrinsic plasticity

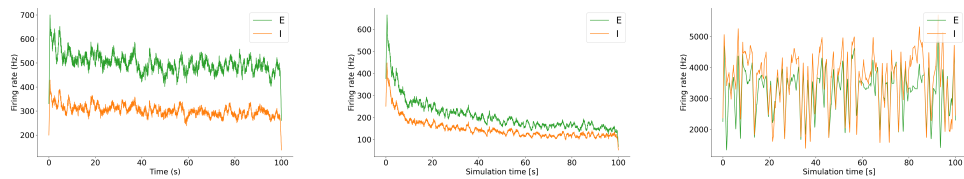


Figure B.9: Population firing rates with IP removed. LIF-SORN left, LIF-SORN-i center, LIF-SORN-c right.

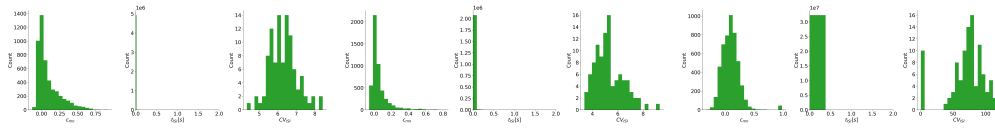


Figure B.10:  $c_{mn}$ , ISI, and CV distributions with IP removed. LIF-SORN left, LIF-SORN-i center, LIF-SORN-c right.

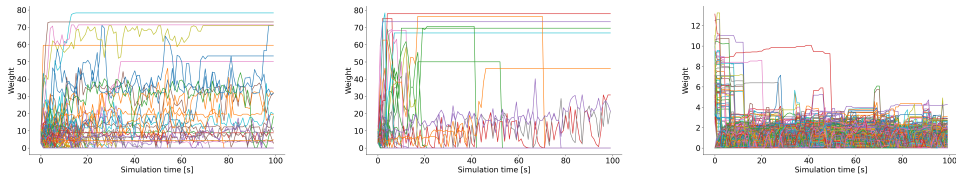


Figure B.11: Recurrent excitatory weight dynamics with IP removed. LIF-SORN left, LIF-SORN-i center, LIF-SORN-c right.

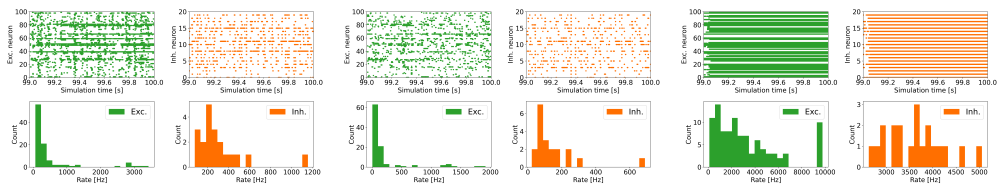


Figure B.12: E/I spike trains and firing rate distributions with IP removed. LIF-SORN left, LIF-SORN-i center, LIF-SORN-c right

## B.4 No spike-timing plasticity

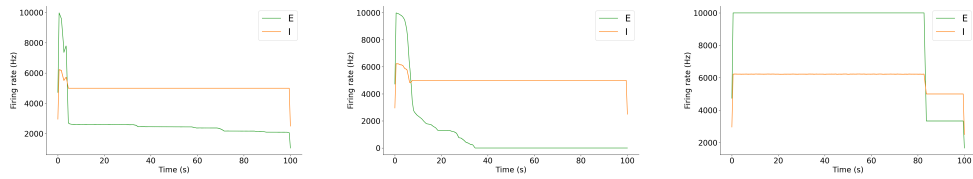


Figure B.13: Population firing rates with STP removed. LIF-SORN left, LIF-SORN-i center, LIF-SORN-c right.

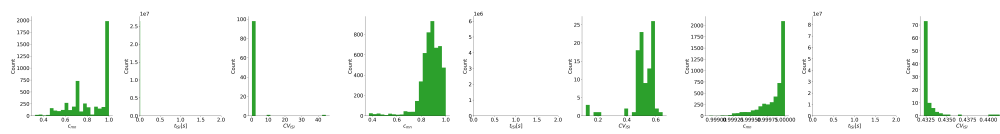


Figure B.14:  $c_{mn}$ , ISI, and CV distributions with STP removed. LIF-SORN left, LIF-SORN-i center, LIF-SORN-c right.

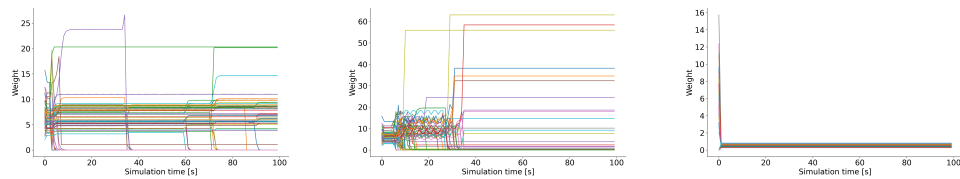


Figure B.15: Recurrent excitatory weight dynamics with STP removed. LIF-SORN left, LIF-SORN-i center, LIF-SORN-c right.

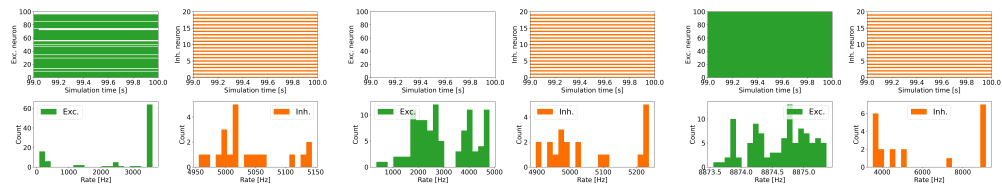


Figure B.16: E/I spike trains and firing rate distributions with STP removed. LIF-SORN left, LIF-SORN-i center, LIF-SORN-c right

# Appendix C

## Evoked network behaviour

### C.1 Baseline

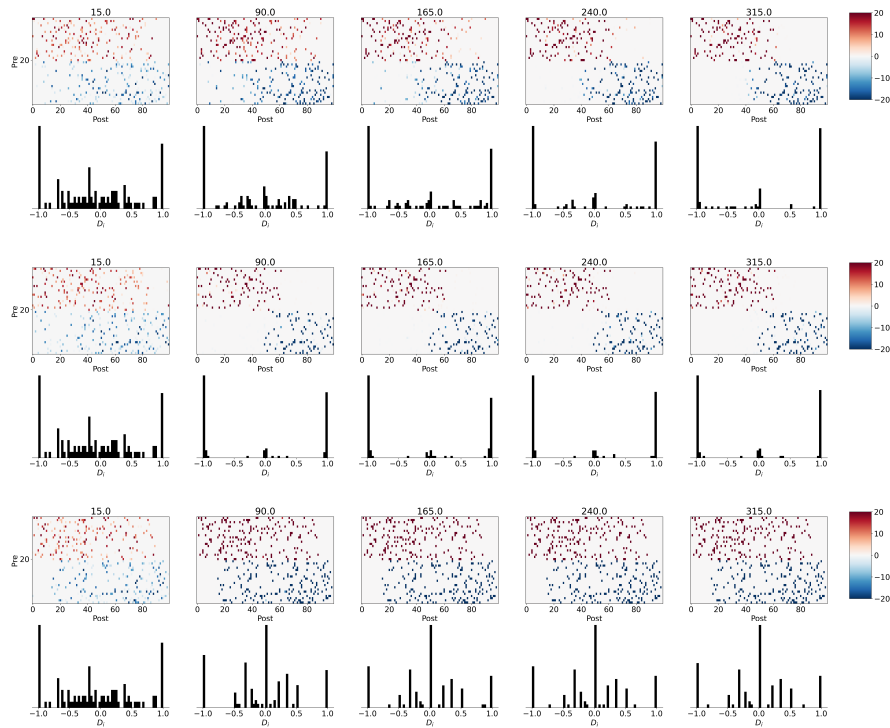


Figure C.1: Baseline input synapse matrices and corresponding E neurons preference score distributions over time. LIF-SORN left, LIF-SORN-i center, LIF-SORN-c right.

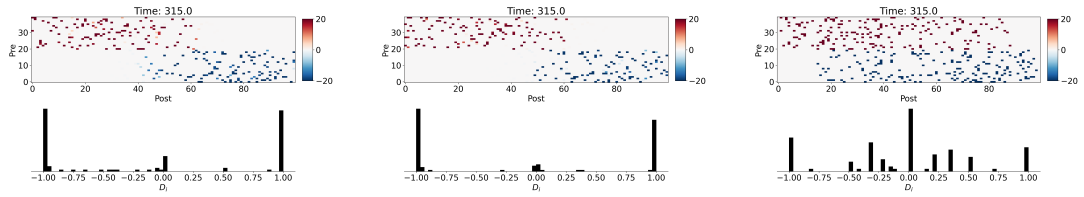


Figure C.2: Baseline input synapse matrices and corresponding E neurons preference score distributions at simulation end. LIF-SORN left, LIF-SORN-i center, LIF-SORN-c right.

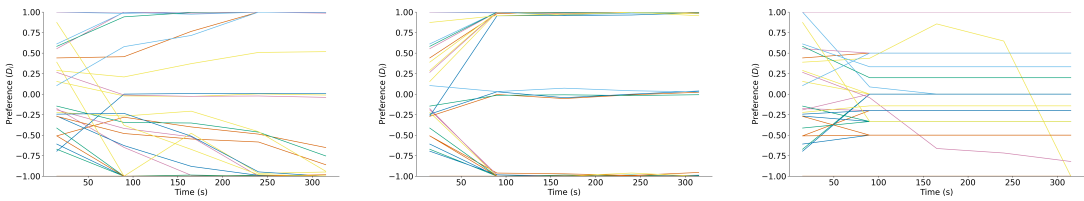


Figure C.3: Baseline E neuron preferences over time. LIF-SORN left, LIF-SORN-i center, LIF-SORN-c right.

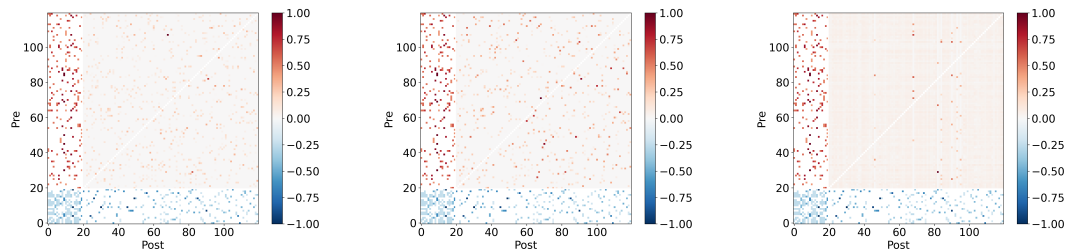


Figure C.4: Baseline recurrent weight matrices at simulation end. LIF-SORN left, LIF-SORN-i center, LIF-SORN-c right.

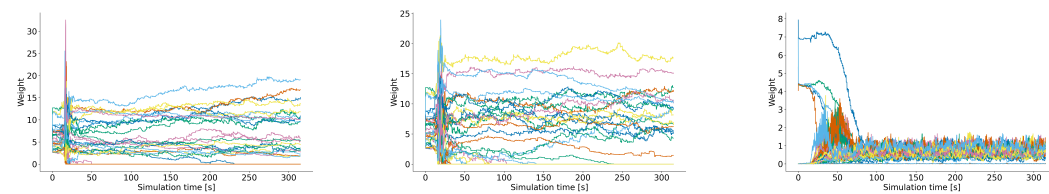


Figure C.5: Baseline recurrent E weight dynamics. LIF-SORN left, LIF-SORN-i center, LIF-SORN-c right.

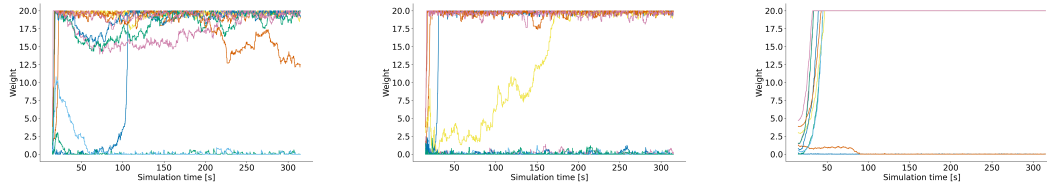


Figure C.6: Baseline input weight dynamics. LIF-SORN left, LIF-SORN-i center, LIF-SORN-c right.

## C.2 No synaptic normalization

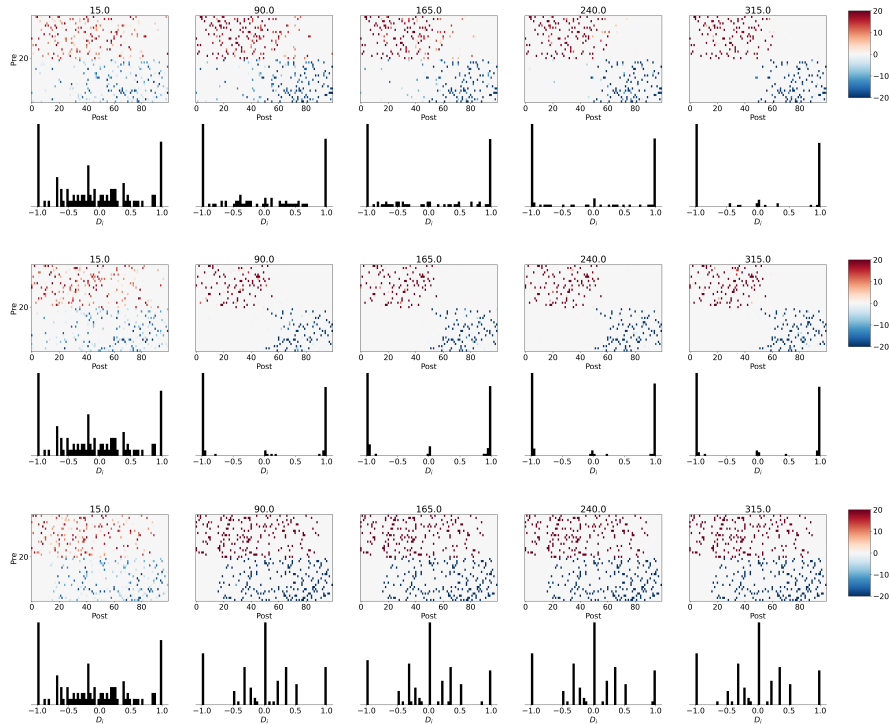


Figure C.7: Input synapse matrices and corresponding E neurons preference score distributions over time with SN removed. LIF-SORN left, LIF-SORN-i center, LIF-SORN-c right.

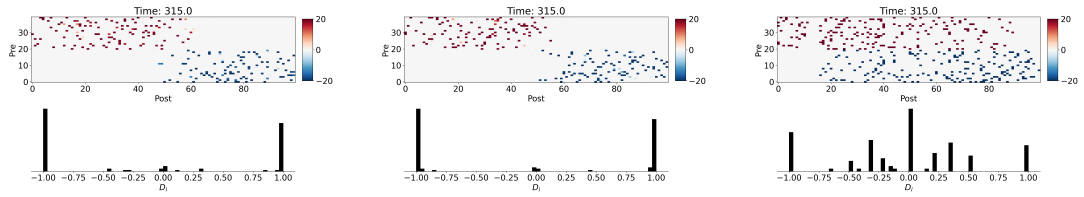


Figure C.8: Input synapse matrices and corresponding E neurons preference score distributions at simulation end with SN removed. LIF-SORN left, LIF-SORN-i center, LIF-SORN-c right.

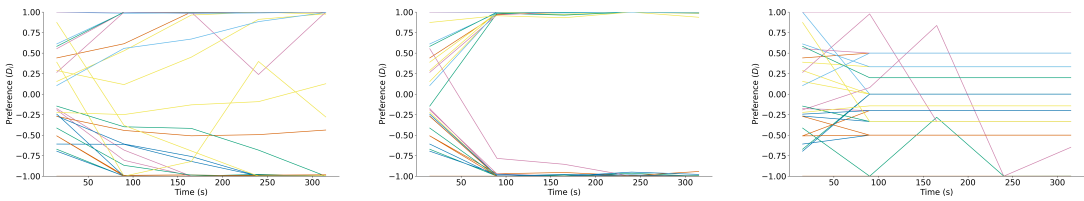


Figure C.9: E neuron preferences over time with SN removed. LIF-SORN left, LIF-SORN-i center, LIF-SORN-c right.

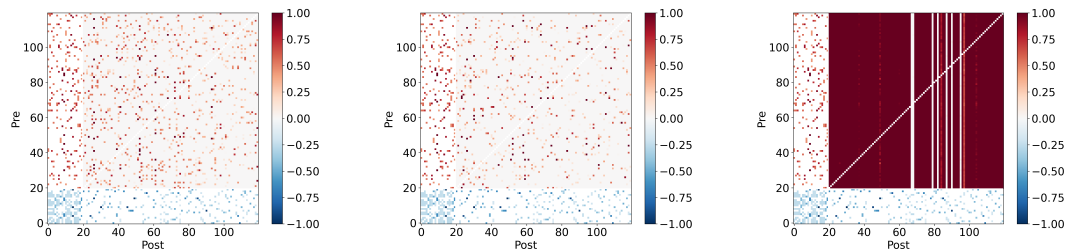


Figure C.10: Recurrent weight matrices at simulation end with SN removed. LIF-SORN left, LIF-SORN-i center, LIF-SORN-c right.

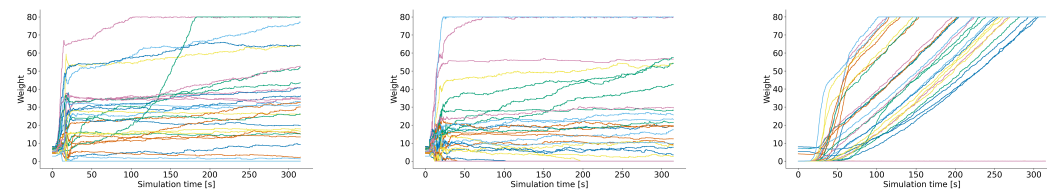


Figure C.11: Recurrent E weight dynamics with SN removed. LIF-SORN left, LIF-SORN-i center, LIF-SORN-c right.

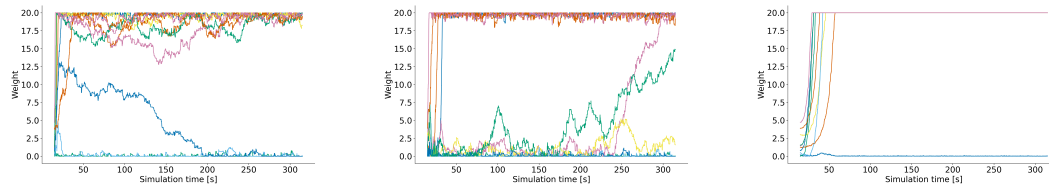


Figure C.12: Input weight dynamics with SN removed. LIF-SORN left, LIF-SORN-i center, LIF-SORN-c right.

### C.3 No intrinsic plasticity

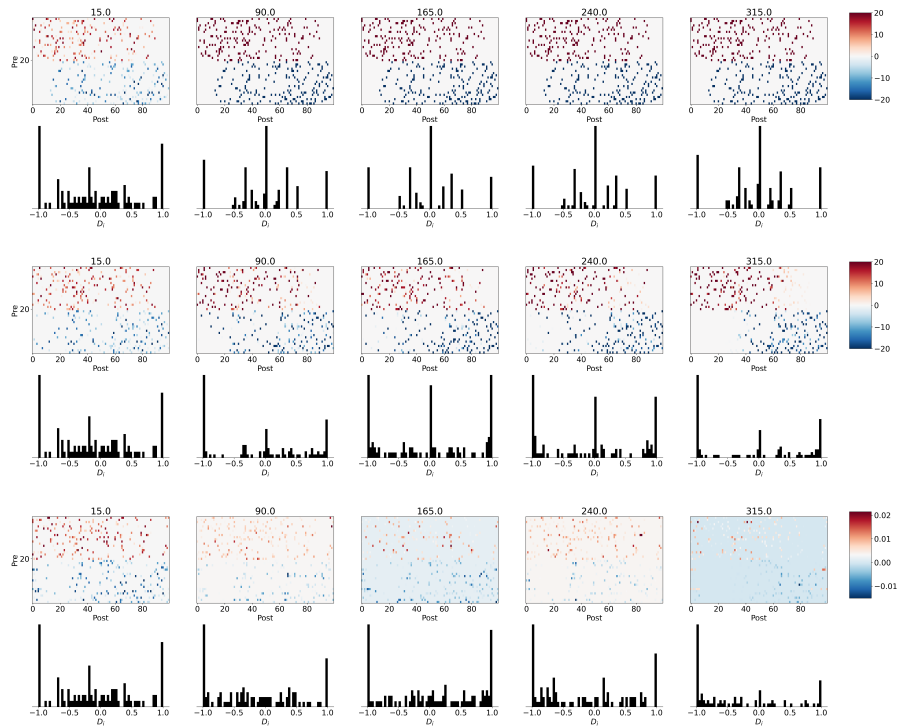


Figure C.13: Input synapse matrices and corresponding E neurons preference score distributions over time with IP removed. LIF-SORN left, LIF-SORN-i center, LIF-SORN-c right.

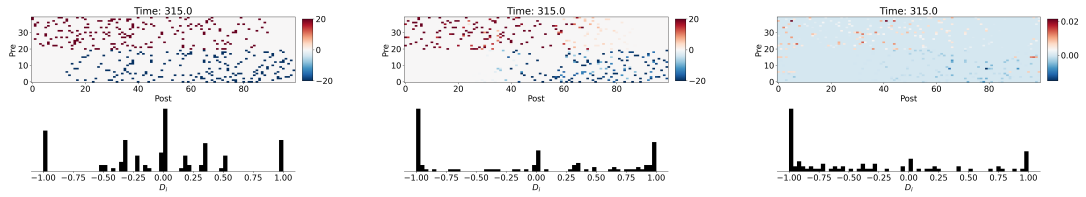


Figure C.14: Input synapse matrices and corresponding E neurons preference score distributions at simulation end with IP removed. LIF-SORN left, LIF-SORN-i center, LIF-SORN-c right.

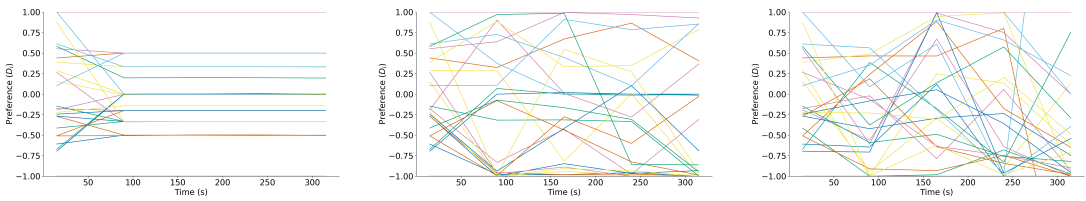


Figure C.15: E neuron preferences over time with IP. LIF-SORN left, LIF-SORN-i center, LIF-SORN-c right.

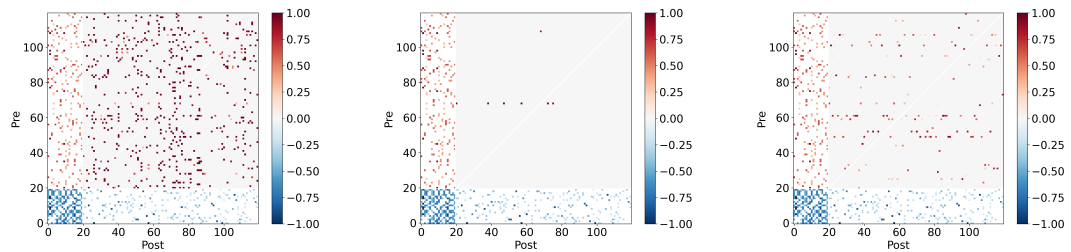


Figure C.16: Recurrent weight matrices at simulation end with IP removed. LIF-SORN left, LIF-SORN-i center, LIF-SORN-c right.

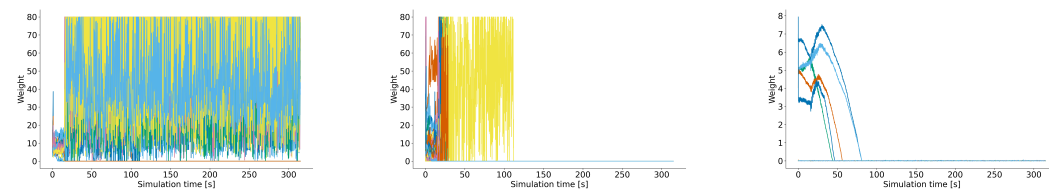


Figure C.17: Recurrent E weight dynamics with IP removed. LIF-SORN left, LIF-SORN-i center, LIF-SORN-c right.

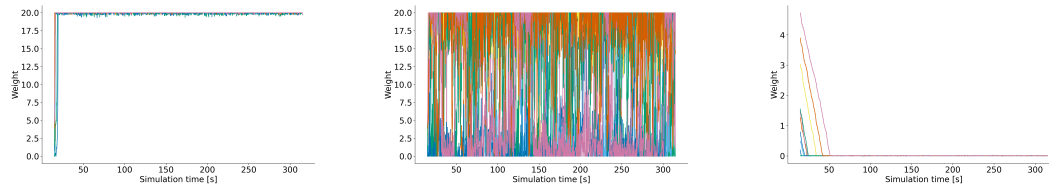


Figure C.18: Input weight dynamics with IP removed. LIF-SORN left, LIF-SORN-i center, LIF-SORN-c right.

## C.4 No spike-timing plasticity

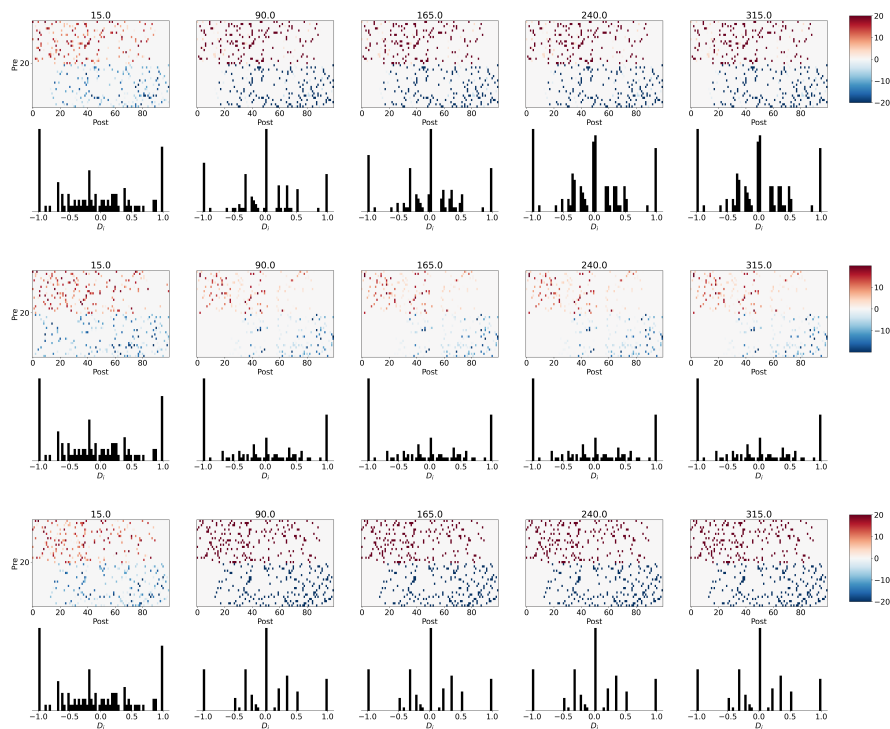


Figure C.19: Input synapse matrices and corresponding E neurons preference score distributions over time with STP removed. LIF-SORN left, LIF-SORN-i center, LIF-SORN-c right.

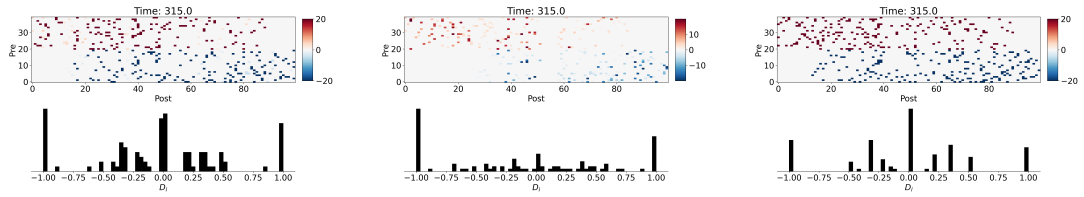


Figure C.20: Input synapse matrices and corresponding E neurons preference score distributions at simulation end with STP removed. LIF-SORN left, LIF-SORN-i center, LIF-SORN-c right.

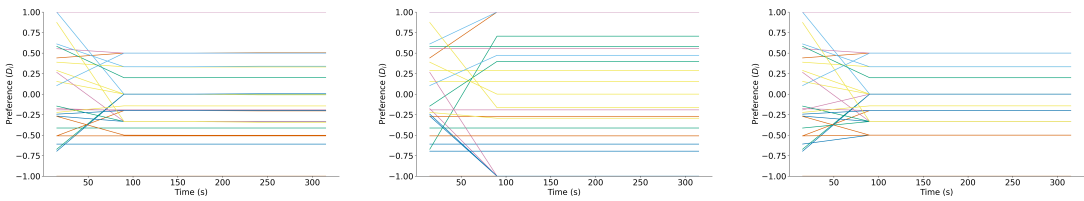


Figure C.21: E neuron preferences over time with STP removed. LIF-SORN left, LIF-SORN-i center, LIF-SORN-c right.

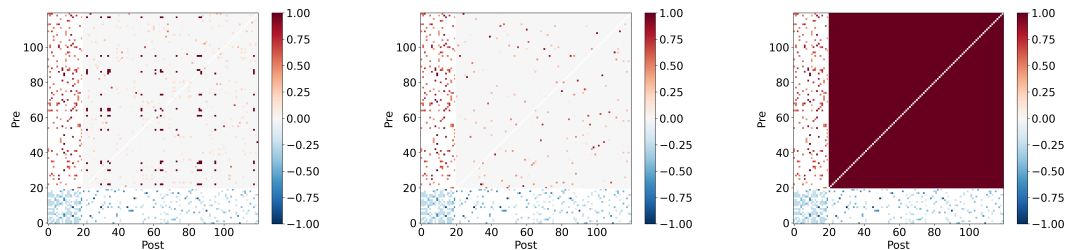


Figure C.22: Recurrent weight matrices at simulation end with STP removed. LIF-SORN left, LIF-SORN-i center, LIF-SORN-c right.

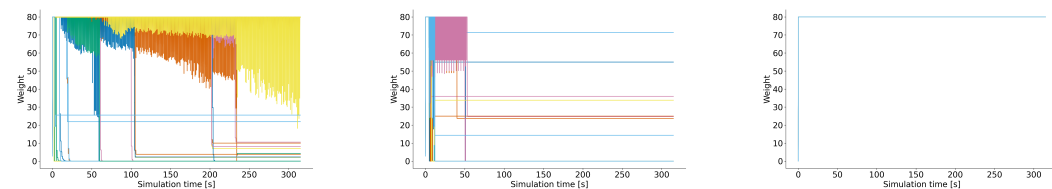


Figure C.23: Recurrent E weight dynamics with STP removed. LIF-SORN left, LIF-SORN-i center, LIF-SORN-c right.

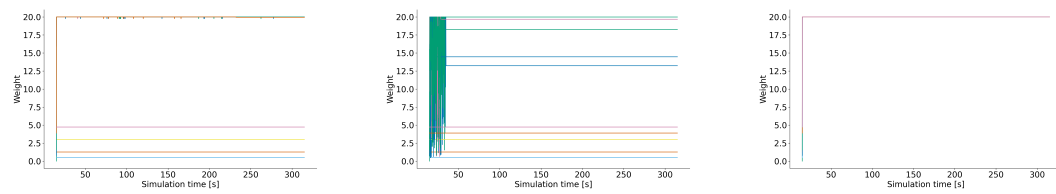


Figure C.24: Input weight dynamics with STP removed. LIF-SORN left, LIF-SORN-i center, LIF-SORN-c right.